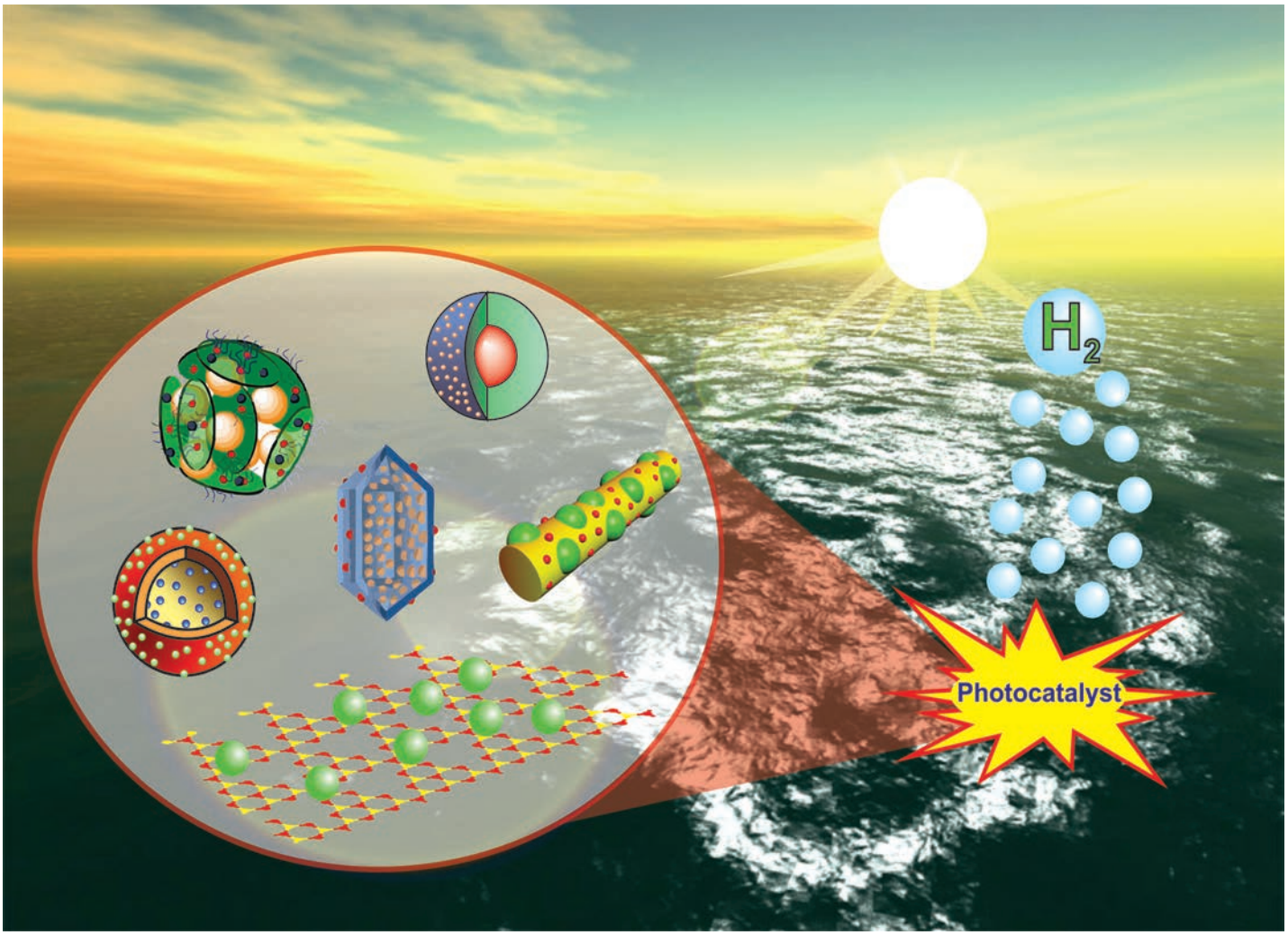

Showcasing research from Nanomaterials & Photocatalysis Lab of the Department of Chemical Engineering, Laval University, Quebec, Canada.

Nanocomposite heterojunctions as sunlight-driven photocatalysts for hydrogen production from water splitting

Hydrogen production *via* photocatalytic water splitting using sunlight has an enormous potential to solve the worldwide energy and environmental crisis. Making multicomponent heterojunctions of different semiconductor nanocomposites offers an effective tool to extend sunlight absorption and also to increase charge carrier lifetimes by enhancing charge separation. Nanostructured photocatalysts can improve the efficiency by providing a large surface area and nanoparticle size. This work reviews advanced heterojunction semiconductors which are activated for hydrogen production under sunlight irradiation.

As featured in:

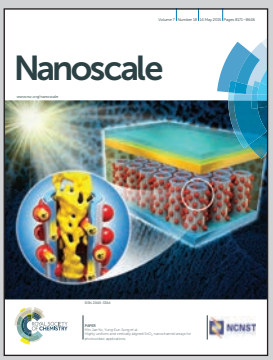

See Trong-On Do *et al.* *Nanoscale*, 2015, **7**, 8187.

ROYAL SOCIETY OF CHEMISTRY

www.rsc.org/nanoscale

Registered charity number: 207890

Nanoscale

REVIEW

Cite this: *Nanoscale*, 2015, **7**, 8187

Nanocomposite heterojunctions as sunlight-driven photocatalysts for hydrogen production from water splitting

Mohammad Reza Gholipour,[a] Cao-Thang Dinh,[a] François Béland[b] and Trong-On Do*[a]

Hydrogen production *via* photocatalytic water splitting using sunlight has enormous potential in solving the worldwide energy and environmental crisis. The key challenge in this process is to develop efficient photocatalysts which must satisfy several criteria such as high chemical and photochemical stability, effective charge separation and strong sunlight absorption. The combination of different semiconductors to create composite materials offers a promising way to achieve efficient photocatalysts because doing so can improve the charge separation, light absorption and stability of the photocatalysts. In this review article, we summarized the most recent studies on semiconductor composites for hydrogen production under visible light irradiation. After a general introduction about the photocatalysis phenomenon, typical heterojunctions of widely studied heterogeneous semiconductors, including titanium dioxide, cadmium sulfide and graphitic carbon nitride are discussed in detail.

Received 6th December 2014,
Accepted 22nd February 2015

DOI: 10.1039/c4nr07224c

www.rsc.org/nanoscale

1. Introduction

Nowadays, fossil fuels play an important role in human life and provide for worldwide energy demands because of their low cost and availability. They are formed from prehistoric fossils over hundreds of years and are no longer available once used. Moreover, the combustion of these fossil fuels produces large quantities of air pollution gases such as nitrogen oxides, sulfur oxides and carbon oxides annually, which cause severe health problems for humans and global climate change. Finding renewable, clean and carbon-neutral alternative energy sources is thus urgently needed.

Among various available renewable energy sources, solar energy is by far the most abundant one. It is estimated that

[a]*Department of Chemical Engineering, Université Laval, Québec, Canada G1V 0A6. E-mail: Trong-On.Do@gch.ulaval.ca*
[b]*SiliCycle Inc., 2500, Boul. du Parc-Technologique, Québec (QC), Canada G1P 4S6*

Mohammad Reza Gholipour

Mohamad Reza Gholipour obtained his BSc and MSc degrees in chemical engineering from Shiraz University, in 2009 and 2012, respectively. He is currently working for his PhD degree at Laval University, Canada under the supervision of Prof. Trong-On Do. He focuses on the synthesis and development of nanocomposite photocatalysts for water splitting via *solar energy.*

Cao-Thang Dinh

Cao-Thang Dinh studied chemical engineering at Laval University under the guidance of Prof. Trong-On Do where he received his Masters in 2011 and PhD in 2014. After graduation, he joined Prof. Edward Sargent's group at the University of Toronto as a Postdoctoral Fellow. He received his BSc at Hanoi University of Mining and Geology in 2004. He worked at Vietnam Academy of Science and Technology from 2005 to 2008. Cao-Thang's current research focuses on the synthesis of multi-functional photocatalysts for the production of solar fuels from water and carbon dioxide.

around 0.01% of the energy of one second of sunlight irradiation is sufficient for the annual energy consumption of human society.[1,2] However, a significant challenge is to put this kind of energy into use and store it for later application. One of the promising ways is using hydrogen as an energy carrier in order to store solar energy in the form of the chemical bond between two atoms of hydrogen. This hydrogen molecule can then react with oxygen in the air to release its energy and produce water as a by-product, which is totally clean for the environment.

Water is the most plentiful supply of hydrogen that can be used to produce hydrogen *via* photocatalytic water splitting. Thus, hydrogen production by means of a photocatalyst, solar energy and water has noticeably attracted attention in recent decades. This technology is clean because it uses photon energy and water. Besides this, it doesn't produce any dangerous by-products or pollutants. Therefore, the photocatalysis process is expected to make a great contribution to energy and environmental challenges in the near future.

The most challenging task in photocatalytic water splitting is to develop efficient photocatalysts which are capable of absorbing sunlight to split water. In general, photocatalysis involves three processes: the excitation, bulk diffusion and surface transfer of photoinduced charge carriers. Thus, an efficient photocatalyst must satisfy several critical requirements related to its semiconducting and chemical properties, its crystalline structure and surface characteristics. However, there are always inherent deficiencies in the semiconductors, and it is very difficult to find a single component that can address all of these requirements. Thus, although many different semiconductors for water splitting have been developed in the last few decades, most of them are activated under UV light and need sacrificial reagents to produce hydrogen from water. It seems that a single-component photocatalyst, even with cocatalysts, cannot obtain a desirable quantum efficiency.

A semiconductor/semiconductor heterojunction, formed by the direct contact of two semiconductors, represents an effective architecture for overcoming the limit of single-component photocatalysts. When two semiconductors with suitable band edge positions are combined, the charge transfer between them can increase the lifetime of the charge carriers, thus promoting the photocatalytic process. In addition, when the band gap of the coupled semiconductor is small, the energy range of photo-excitation for the system is also extended. In this review paper, we summarize various nanocomposite photocatalysts which were active for hydrogen production under visible light illumination.

2. Fundamentals of photocatalytic water splitting

Fujishima and Honda were pioneers in decomposing water with light illumination.[3] They discovered that TiO_2 and Pt can act as the anode and cathode electrodes, respectively, in a photoelectrochemical cell. This system could split water into hydrogen and oxygen under intense UV irradiation. Some years later, Bard applied the concept of this system to introduce a photocatalysis process.[4] Since then, there have been enormous efforts in developing semiconductors that can decompose water into H_2 and O_2 under illumination with light.

Generally, photocatalytic water splitting with sunlight consists of three main steps: (I) a semiconductor absorbs light photons and generates excited electrons and holes; (II) these

François Béland

Francois Béland is currently the Vice President of R&D at SiliCycle. He earned his Ph.D. in 1999 from Laval University in Quebec City where he studied silica-based catalysts by different spectroscopy methods. Francois then traveled to the South of France for his post-doctoral studies at the Ecole Nationale Supérieure de Chimie de Montpellier. There he studied different catalytic reactions in organic chemistry catalyzed by silica-based heterogeneous catalysts. After his post-doc work, he started his career at SiliCycle as a researcher. After his promotion to R&D Director, his focus was to develop the SiliaBond (functionalized silica gels) product line. Dr Béland has 15 years of experience with silica-based products for different applications in chromatography and organic chemistry.

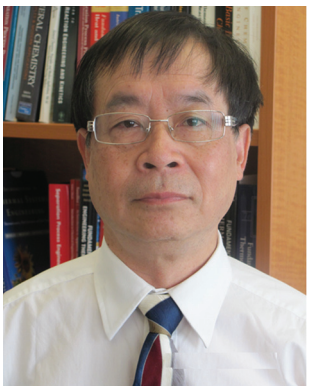

Trong-On Do

Trong-On Do is a full professor in the Department of Chemical Engineering at Laval University, Canada. He received his MSc in 1986 and PhD in 1989 at University of P. and M. Curie (Paris 6, France). After a period at Brunel University (UK) and the French Catalysis Institute (France), he moved to Laval University in 1990. He then spent two years 1997–1999 in Profs. Hashimoto/Fujishima's group at Kanagawa Academy of Science and Technology under the Japanese STA Fellowship Award before re-joining Laval University as a professor associated with the NSERC Industrial chair. He has published over 120 papers and review articles in refereed journals and holds 5 international patents. He is the recipient of the 2014 Canadian Catalysis Lectureship Award (CCLA).

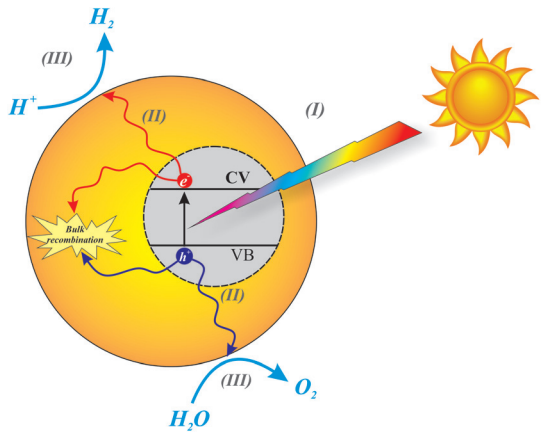

Fig. 1 Schematic of the fundamental mechanisms of photocatalytic water splitting.

excited electrons and holes can migrate to the surface of the semiconductor or recombine again inside the bulk material; (III) on the surface, holes can oxidize water to O_2 (eqn (1)) and electrons can reduce protons to H_2 (eqn (2)). Fig. 1 illustrates schematically the main steps in water splitting.

$$H_2O + 2h^+ \rightarrow \frac{1}{2}O_2 + 2H^+ \quad (1)$$

$$2H^+ + 2e^- \rightarrow H_2 \quad (2)$$

The semiconductor band gap determines which wavelength of sunlight can be absorbed. A semiconductor with a wide band gap (E_{bg} > 3 eV) can only absorb UV light, which approximately accounts for 5% of solar energy. In contrast, a narrow band gap semiconductor (E_{bg} < 3 eV) can be activated by visible light irradiation, which constitutes 43% of the sunlight spectrum. Besides the band gap, the positions of the valence and conduction bands are also very important in photocatalytic water splitting. For H_2 evolution, the conduction-band edge should be more negative than the reduction potential of H^+ to H_2 (E_{H^+/H_2} = 0 V *vs.* NHE at pH = 0). On the other hand, the valence-band edge should be more positive than the oxidation potential of water (E_{O_2/H_2O} = 1.23 V *vs.* NHE at pH = 0) in order to evolve oxygen. Therefore, the band gap of the semiconductor should be at least 1.23 eV in order to split the water. The equivalent light wavelength for this band gap energy is 1100 nm, which is in the near-infrared region of the sunlight spectrum. By considering other factors such as energy losses during different stages in the photocatalytic process, effective semiconductors should have band gaps greater than 2 eV, which is related to light with wavelength less than 620 nm.[5,6] Although some semiconductors can absorb infrared light by a photon up-conversion mechanism, their applications are usually limited to the degradation of organic compounds.[7–10]

2.1. Overall water splitting

The decomposition of water directly into hydrogen and oxygen under sunlight irradiation is the ultimate goal of a photocatalytic hydrogen generation system. In this process, a semiconductor with proper band-edges can absorb photon energy and evolve hydrogen and oxygen simultaneously. However, this reaction is thermodynamically non-spontaneous, with a Gibbs free energy of 237 kJ mol^{-1}.[11]

$$2H_2O \overset{\text{photon energy}}{\Rightarrow} 2H_2 + O_2 \quad (3)$$

Some semiconductors can absorb UV light and split water directly into hydrogen and oxygen, but most of them have an energy conversion efficiency of less than 1%.[12–14] Moreover, they cannot produce hydrogen and oxygen in a stoichiometric ratio because one type of charge carrier is accumulated on the surface of the photocatalyst.[11] One exceptional example is a GaN–ZnO solid solution photocatalyst that can split water into hydrogen and oxygen stoichiometrically under visible light illumination with a quantum efficiency of about 6%.[15] It is obvious that overall water splitting is very difficult to carry out under visible light illumination and has become one of the greatest challenges for researchers in this field.

2.2. Sacrificial reagent systems

As discussed earlier, overall water splitting is a very hard reaction to carry out, and it needs a specific kind of semiconductor with appropriate band edge positions. Nevertheless, some semiconductors can do one of the half reactions of water splitting, *i.e.* water reduction or oxidation, in the presence of suitable sacrificial reagents (electron donors or acceptors). In principle, sacrificial agents usually react with one type of charge carrier while the other carrier reacts with water to produce hydrogen or oxygen. Electron donors, which consume excited holes on the surface of the semiconductor, are used for the water reduction half reaction and electron acceptors (electron scavengers) are usually needed for water oxidation, as illustrated in Fig. 2. Generally, the electron donors must be more readily oxidized than water by excited holes, while the electron acceptors must be more readily reduced than water by excited electrons. The most common electron donors are methanol, ethanol, triethanolamine (TEA) and an aqueous

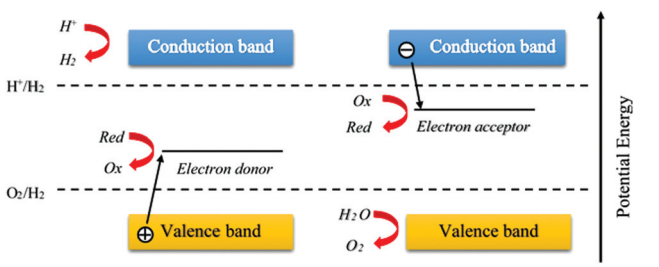

Fig. 2 Schematic of the principles of water reduction or oxidation in the presence of sacrificial reagents.

solution of Na_2S–Na_2SO_3, whereas metal cations such as Ag^+ and Fe^{3+} are usually utilized as electron acceptors.[11]

Various mechanisms have been proposed to explain the consumption of sacrificial reagents in hydrogen production reactions.[14,16] These electron donors react more easily with holes than water due to its less positive oxidation potential. This would lead to accelerated hole consumption on the surface of the photocatalyst and so the positive charge accumulation is partially prevented and, as a result, protons and photoexcited electrons can react together more easily. It should be noted that, in the case of using methanol as the electron donor, hydrogen is also produced from water as a result of methanol conversion (eqn (4)).[17,18] However, by increasing the carbon chain, the contribution to H_2 production from alcohol conversions decreases substantially.[18] Moreover, Guzman showed that the direct reaction of methanol with holes does not proceed to an appreciable extent in the presence of a high concentration of water.[19]

$$CH_3OH + H_2O \rightarrow CO_2 + 3H_2 \quad (4)$$

Semiconductors capable of decomposing water in the presence of sacrificial agents may seem to be useless. Nevertheless, these photocatalysts can not only be used in the Z-schematic system but also some of them can be used to produce H_2 using biomass-derived sacrificial reagents.[20,21]

2.3. Electron mediator systems

The electron mediator system is also called the Z-scheme system or a dual photocatalyst system. The concept of this system is to transfer charge carriers using two different electron mediators in a solution; after participating in redox reactions, they all return to their original chemical states.[22] This procedure for overall water splitting is entirely different to the two previous methods. It needs two different photocatalysts: a semiconductor providing photoexcited electrons to participate in the half-reaction for H_2 evolution and another one supplying photogenerated holes to take part in the half-reaction of water oxidation. Moreover, two semiconductors could be excited simultaneously and one half of the charge carrier will recombine in order to bring the electron mediators to their original states (Fig. 3). Some of the most common electron mediators are Fe^{3+}/Fe^{2+}, IO^{3-}/I^- and Ce^{4+}/Ce^{3+}.[23]

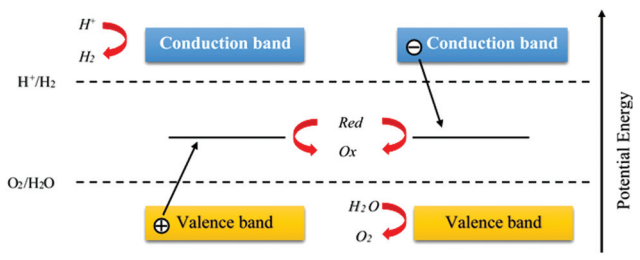

Fig. 3 Schematic of the principles of overall water splitting in the Z-scheme system.

There are some review papers discussing different approaches and applications of this dual-step system, which is similar to plant photosynthesis.[24,25] Nonetheless, this system has some drawbacks in comparison to the one-step system. For instance, Z-scheme systems are usually more complicated and need more photons to produce the same amount of hydrogen because half of the excited charges are used in order to bring the excited mediator to its ground state for further reactions.[22,26]

2.4. Activity and quantum efficiency

Photocatalytic activity depends on many factors such as the light source (Xe or Hg lamps), light intensity, reaction cell, different directions of irradiation (top, inner, or side), reaction media (water or various sacrificial agents), and the quantity of the photocatalyst. The simplest way to find the semiconductor activity is to measure the amount of evolved gases in a specific period of time and report it in μmol h^{-1} or μmol h^{-1} g^{-1} units.[23]

Quantum yield (quantum efficiency) is another way to report the photocatalytic activity of a semiconductor. This is independent of the affecting factors that are mentioned above and is defined as:[27]

$$\text{Quantum yield (\%)} = \frac{\text{Number of reacted electrons}}{\text{Number of absorbed photons}} \times 100 \quad (5)$$

Despite the fact that this equation can give us the accurate quantum yield, it is very hard to measure the real number of absorbed photons. In order to solve this problem, researchers have suggested using the apparent quantum yield, which is defined as follows:[23]

$$\begin{aligned}\text{Apparent quantum yield (\%)} &= \frac{\text{Number of reacted electrons}}{\text{Number of incident photons}} \times 100 \\ &= \frac{2 \times \text{Number of evolved } H_2 \text{ molecules}}{\text{Number of incident photons}} \times 100 \\ &= \frac{4 \times \text{Number of evolved } O_2 \text{ molecules}}{\text{Number of incident photons}} \times 100\end{aligned} \quad (6)$$

It is obvious that the apparent quantum yield is smaller than the real quantum efficiency because of the difference between the number of absorbed photons and incident light.

Solar energy conversion efficiency is a method to calculate solar cell efficiency. It can also be used to report the photocatalytic activity of a semiconductor.

$$\text{Solar energy conversion efficiency (\%)} = \frac{\text{Output energy of } H_2 \text{ evolved}}{\text{Energy of incident solar light}} \times 100 \quad (7)$$

Up to now, semiconductors have had extremely low solar energy conversion values and so this indicator is seldom used.[12] It is anticipated that for industrial application of water splitting *via* sunlight, this efficiency should be noticeably improved.

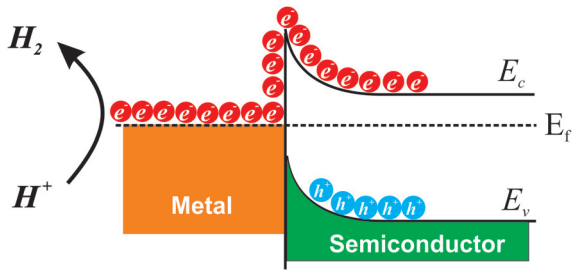

Fig. 4 Schematic of the energy band model of a Schottky junction.

2.5. Cocatalysts

A cocatalyst is a compound added to the photocatalyst semiconductors to improve their activity. In photocatalytic water splitting, the cocatalysts can be used to enhance either the water oxidation or reduction reactions. The cocatalysts for water reduction are usually small metal nanoparticles (NPs) which can form a Schottky junction with semiconductors and enhance charge separation in a photocatalyst or photoelectrochemical cell.[28,29] In principle, the contact between the metal and the semiconductor creates an electric field that separates excited electrons and holes more easily, as demonstrated in Fig. 4.[30–32] If the work function of the metal matches the conduction band-edge of the semiconductor, excited electrons move from the semiconductor to the metal, and from there they can react with water. In addition, the metal provides active sites for hydrogen generation due to its relatively low over-potential for water reduction.

The physical and chemical properties of the cocatalyst such as particle size and valence states, which significantly affect their performance, are strongly dependent on the loading method of the cocatalysts. Although depositing more cocatalyst provides more active sites for reactions, it reduces the absorption ability of the photocatalyst. Therefore, the concentration of the cocatalyst should be optimized to obtain the maximum activity during water splitting under light illumination.

There are two main techniques to deposit cocatalysts onto the surface of semiconductors: *in situ* photodeposition and impregnation. In the first method, the cocatalyst is reduced by photoexcited electrons onto the surface of a semiconductor under light irradiation in the presence of sacrificial reagents. Therefore, the semiconductor should be mixed with a precursor solution of the cocatalyst. If the photo-reduction step is performed subsequently with various precursors, a core–shell structure can be achieved easily.[33]

The second method is usually followed by a post-calcination step. First, a semiconductor is impregnated with a solution containing the cocatalyst precursor and then evaporated and dried. After this stage, the dry mixture is calcined in air or other gases such as hydrogen or argon in order to obtain the desired states of the metal or metal oxide. The final state of the cocatalyst depends on the gas treatment, temperature and the type of precursor used.[23]

There have been great efforts to use different types of cocatalysts including transition metals, metal oxides and noble metals for each half reaction of water splitting. The most common cocatalysts for hydrogen evolution are Pt, Rh, Au, NiO[34] and RuO_2.[34,35–39] Other types, such as a core–shell configuration of the cocatalysts, have been recently proposed to improve H_2 evolution in overall water splitting.[33,40] Although cocatalysts are an important part of the photocatalytic system, in this review we only focus on different nanocomposites of semiconductors that are active under visible light illumination.

3. Nanocomposites for visible-light-driven photocatalytic hydrogen production

It has been proven that some semiconductor properties such as specific surface area, particle size, crystallinity, crystalline phase and morphology have considerable effect on photocatalytic activity.[41] Charge recombination centers are some kind of defect (in the crystal structure or on the surface of photocatalysts) where photoexcited electrons and holes recombine together.[42] Because of this phenomenon, most photocatalysts have very low efficiencies under light irradiation.[43] Even in single crystals (free of defects), the charge recombination process is also possible, due to their non-directional and long-distance migration from the inside to the photocatalyst surface. It is noted that excited electrons and holes recombine together in less than 10^{-9} s, whereas it takes more time for absorbed species to react with these charges (10^{-8}–10^{-3} s).[2] If the recombination process can be partly diminished, highly efficient photocatalysts for the water splitting reaction will be gained.

Scientists have been working on different strategies to enhance charge separation and migration. Nanotechnology has a great advantage for photocatalytic activity due to the fact that the photoexcited charges can migrate considerably shorter distances from the bulk material to the reaction sites on its surface.[7] In addition, the high surface area of nanomaterials results in enhanced chemical adsorption on the surface of the nanoparticles and so the possibility of reactants reacting together is boosted noticeably. For instance, nano-sized CdS, $LaFeO_3$ and Ta_3N_5 revealed higher photocatalytic activities for H_2 evolution than the bulk ones.[44–47] Nevertheless, by reducing the particle size to nanoscale, surface defects and charge recombination become dominant, which compensates for the benefits of nanoparticle semiconductors.[48,49] Therefore, the highest activity was not necessarily achieved with the smallest nanocrystals and so the optimal particle size is a key factor for acquiring the highest efficiency of a nano-photocatalyst.[50,51] It is noteworthy that, in nanomaterials, crystallinity plays a more dominant role than having a higher surface area.[7]

As seen in Fig. 5, the number of publications on nano-photocatalysts has increased substantially in the last decade,

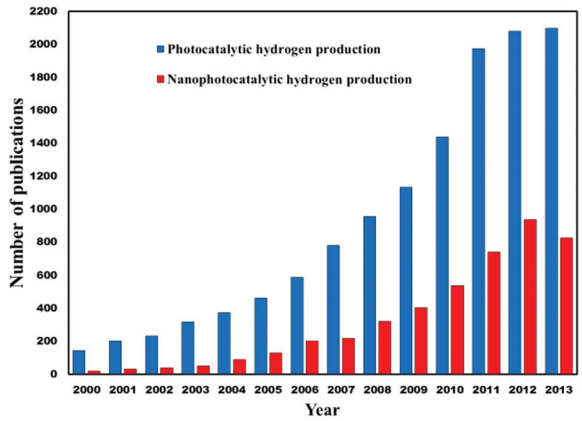

Fig. 5 The number of publications on photocatalytic H_2 production sorted by year. Data were collected from the "Web of Science".

but obviously more work needs to be done in this field in order to find suitable and efficient photocatalysts for hydrogen production.

3.1. Semiconductor heterojunction structures

Instead of using a single semiconductor, combining a semiconductor with other semiconductors, metals, and molecules would lead to the formation of a heterojunction structure between them. These heterojunctions were found to enhance the performance of various devices such as solar cells as well as photoluminescent and electro-chromic devices.[52–54] In addition, the utilization of nanocomposites as photocatalysts instead of single semiconductors is another efficient and practicable approach to enhance the photocatalytic performance. In this kind of nanocomposite, excited charges migrate from one semiconductor to another semiconductor (or metal which acts as a cocatalyst). The second semiconductor should have a proper band-edge position or a higher efficiency in comparison to the first one. Furthermore, this approach can improve the device efficiency due to the fact that the reduction and oxidation reactions happen in two different components.[2]

All heterojunctions can be categorized into three types based on their conduction and valance band positions, as illustrated in Fig. 6. In Type 1, both excited electrons and holes move from semiconductor 2 to semiconductor 1 due to their band edge positions. Usually this kind of heterojunction doesn't improve photocatalysts because of the accumulation of both charge carriers on one semiconductor.

In the second group of heterojunctions, the conduction band of semiconductor 1 is lower than that of semiconductor 2. However, the valence band of semiconductor 1 has higher value than that of semiconductor 2. As a result, excited electrons can move from semiconductor 2 to 1, although generated holes migrate *vice versa*. If both semiconductors have sufficient intimate contacts, an efficient charge separation will occur during light illumination. Consequently, charge recombination is decreased and so charge carriers have a longer lifetime, which results in higher photocatalyst activity. Most of the composites discussed in this review are type 2.

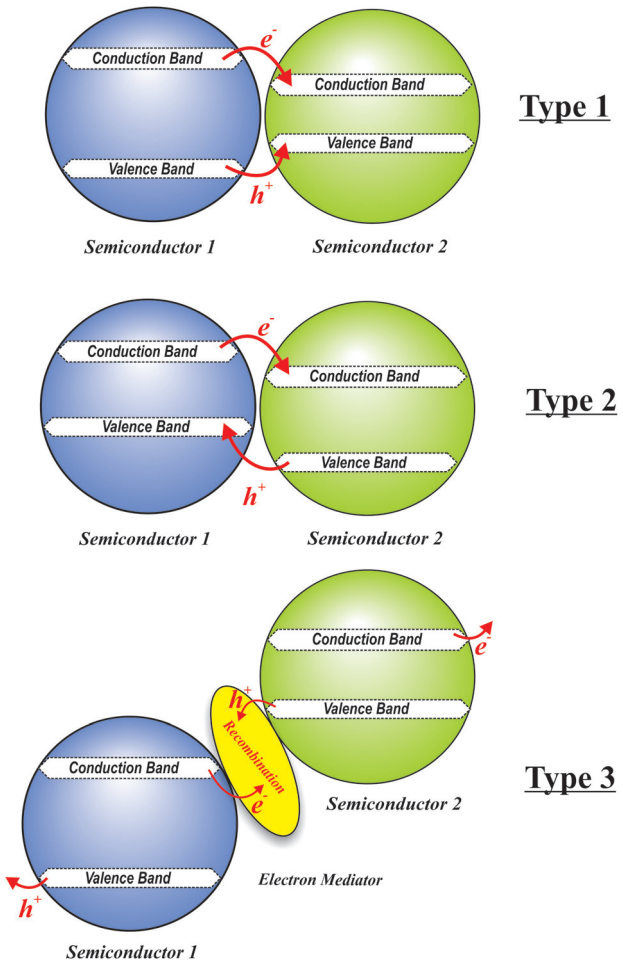

Fig. 6 Various kinds of heterojunctions.

Type 3 consists of semiconductors in which both the valence and conduction bands of one semiconductor are lower than the other, as can be seen in Fig. 6. This kind can be applied in the Z-scheme system with an appropriate electron mediator or some kind of bridge that attaches the two semiconductors. For instance, Wang *et al.* synthesized a core–shell nanocomposite of ZnO–CdS@Cd in such a way that elemental Cd acts as the charge-carrier bridge.[55] A schematic of this nanocomposite is demonstrated in Fig. 7.

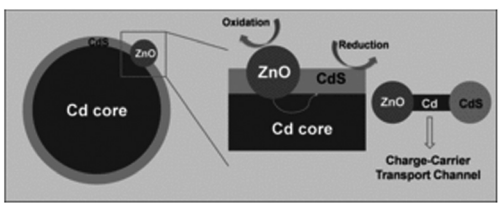

Fig. 7 Scheme of the improved mechanism of photoexcited charge-carrier transport in the ZnO–CdS@Cd heterostructure.[55] Image reproduced with permission from John Wiley and Sons.

3.2. Various kinds of semiconductors

All of the semiconductors can be classified into 3 main groups based on their properties for hydrogen production: metal oxides, metal sulfides, and metal-free semiconductors.

There are different metal oxides that can be utilized as photocatalysts in a variety of reactions according to their band structures and activities. Most of them are active for hydrogen production under UV light irradiation because of their conduction band positions. Among them, titanium dioxide has attracted the most attention from scientists due to its efficiency, high stability, low cost and non-toxicity. However, it can absorb UV light, likewise other metal oxides, due to its wide band gap. Therefore, this semiconductor has a very low energy conversion from sunlight.

Contrary to metal oxides, metal sulfides usually have narrow band gaps and so they can absorb the energy of photons in the visible region. In addition, the conduction band of these semiconductors is more negative than the reduction potential of water and so they can reduce water to hydrogen. Nevertheless, these semiconductors usually consume generated holes to oxidize themselves. Thus, they are unstable during photocatalytic reactions. CdS is one of the best semiconductors with a high efficiency for hydrogen production under sunlight irradiation. Due to its instability, the metal sulfide is combined with other semiconductors with the aim of improving its stability and photocatalytic efficiency.

Besides these semiconductors, some nitrides also show photo-activity for hydrogen production in the visible range of the sunlight spectrum. Recently, graphitic carbon nitride has attracted a lot of interest because of its special properties such as its relatively narrow band gap and non-toxicity. This metal free polymer shows hydrogen production under visible light irradiation with high stability. However, its conversion efficiency is lower than that of TiO_2 or CdS and so further efforts need to be made in order to increase its efficiency. We will discuss different structures and compositions of these photocatalysts in detail, which shows hydrogen activity under visible light irradiation.

3.3. Titanium dioxide-based nanocomposites

Titanium dioxide typically has three crystal phases: anatase, rutile and brookite, among which anatase exhibits both high stability and high photocatalytic activity. The crystal structure of anatase and rutile are tetragonal, however brookite is orthorhombic.[56,57] Various forms of TiO_2 have slightly different band gaps of around 3 eV, due to the variety in the crystal structures. Rutile is the thermodynamically stable form, and brookite does not usually show appreciable photocatalytic activity, but anatase is often indicated as the most active phase. The conduction band of TiO_2 is slightly higher than the reduction potential of water and so it can reduce protons when it is excited by light.

Some researchers synthesized nanocomposites of TiO_2 and some metal oxides, which are activated in the visible light region.[58–66] Interestingly, some of them showed higher hydrogen production in comparison to pristine TiO_2 due to visible light absorption and better charge separation. For instance, Martha *et al.* tried to increase hydrogen production by combining doped TiO_2 with V_2O_5.[61] Although N,S-doped TiO_2 has a very low hydrogen evolution, the combination of the doped TiO_2 with V_2O_5 exhibited 7 times higher hydrogen production under visible light irradiation (296.6 μmol h^{-1}). Xie *et al.* showed that a nanocomposite of $TiO_2/BiVO_4$ had a much longer lifetime of photoexcited charge carriers and so a higher charge separation.[65] The main reason for this phenomenon is related to high movements of photoexcited electrons from $BiVO_4$ to TiO_2. Due to this reason, this photocatalyst had unexpected visible light activity for water splitting in contrast to $BiVO_4$, which was almost inactive in this region. They reported that $TiO_2/BiVO_4$ with a molar ratio of 5%, could evolve 2.2 mol h^{-1} hydrogen, which was much higher than mixing with reduced graphene oxide nanosheets (0.75 mol h^{-1}) under similar conditions.[66] Another group deposited Fe–TiO_2 nanoparticles (FTO) on the surface of $CaIn_2O_4$ nanorods (CIO).[63] This nanocomposite revealed hydrogen production in the presence of KI as a sacrificial agent and Pt as a cocatalyst. The contact of these two nanoparticles facilitated charge separation and led to greater hydrogen evolution. This nanocomposite exhibited H_2 production at a rate of 280 μmol h^{-1} g^{-1}, which was 12.3 and 2.2 times higher than $CaIn_2O_4$ and Fe–TiO_2, respectively. Due to the synthesis method (physical mixing of FTO and CIO), there is no control to give a uniform dispersion of FTO on CIO. In addition, the cocatalyst should be deposited on FTO in order to be more effective for hydrogen production. It seems that by applying some coating methods, the activity of this nanocomposite can improve, to even more than 280 μmol h^{-1} g^{-1}.

It is worth mentioning that iron oxide is capable of use in metal organic frameworks (MOFs) in diverse morphologies with titanium oxide.[67–69] For instance, Lin's group created a nanocomposite of mixed metal oxides (Fe_2O_3 and TiO_2) *via* MOF templates.[67] They used a MIL-101 MOF (Fe source) to deposit amorphous TiO_2 and after deposition they calcined the mixture in order to acquire the Fe_2O_3/TiO_2 nanocomposite. As a result, crystalline octahedral nano-shells were obtained which could produce hydrogen under visible light irradiation. Although TiO_2 is only active under UV light and Fe_2O_3 has a more positive conduction band than the reduction potential of H_2, this novel nanocomposite with the help of Pt metal as a cocatalyst produced 30.0 μmol g^{-1} of hydrogen in 48 hours in the presence of TEA as a sacrificial agent. The reason for this weird activity is that some iron ions from MIL-101 can be doped into the TiO_2 crystallinity during the calcination process and the others converted into Fe_2O_3. Fe_2TiO_5 and Ti-doped Fe_2O_3 are both considered to be active photocatalysts under visible light in H_2 formation because of their small band gaps (Fe_2TiO_5 = 2.2 eV and Ti-doped Fe_2O_3 = 2.1 eV) and the edge of their conduction bands, which are more negative than H^+ reduction.[68] Moreover, further characterizations showed that this material was stable during hydrogen evolution and no decrease in activity was observed. By introducing

this kind of hollow nanostructure, the surface area of the photocatalyst increased significantly, resulting in higher activity owing to more available active sites. Another example of this type was developed in our group. We proposed a new route to prepare a novel type of photocatalytic hollow Fe_2O_3–TiO_2 nanostructure using the metal organic framework (MOF) structure consisting of coordinatively unsaturated metal centers (namely, MOF-UMCs) as a hard template.[69] In this type of MOF-UMCs material, each trimeric Fe(III) center possesses terminal water molecules that can be removed by vacuum and temperature treatments to generate Lewis acid sites, to which the amine group of the titanium precursor can be grafted *via* the lone electron pair of the nitrogen atom for the preparation of a core/titania shell nanostructure, as illustrated in Fig. 8. The achieved hollow nanostructure of the Fe_2O_3–TiO_2–PtO_x photocatalyst possesses two distinct cocatalysts which are deposited separately on two sides of its hollow surface. The distance between two cocatalysts (wall thickness of the template) was 15–35 nm, which strongly facilitated charge separation and so increased photocatalytic activity. One of the cocatalysts was created from metal clusters of the MOF after calcination, located inside the hollow structure and the other was made from metal doping (PtO_x) onto the surface of this nanocomposite. Interestingly, the visible light absorption band edge extended to 610 nm. Under visible light illumination and in the presence of lactic acid, this nanocomposite could produce 22 μmol h^{-1} hydrogen without any reduction in its activity even after 5 cycles. The total amount of H_2 after five cycles was 110 μmol under visible light irradiation. Although this amount of hydrogen production was not so much in comparison to other photocatalysts, this approach may be used to develop other hollow structures with higher activity for hydrogen evolution in the visible light region.

In addition to metal oxides, scientists tried to mix diverse metal sulfides with titanium oxide due to their higher visible light absorption. CdS is the best metal sulfide to combine with TiO_2 because of its appropriate conduction band and higher efficiency. Due to the importance of this kind of nanocomposite, different compositions and morphologies will be discussed thoroughly in another section. Here, other metal sulfide composites with TiO_2 are explained in detail.[70–74] It was reported that the single nanoparticles of In_2S_3 or Pt/TiO_2 were not active towards H_2 formation under visible light irradiation. However, the combined In_2S_3/Pt/TiO_2 nanostructure produced H_2 under visible light at the rate of 135 μmol h^{-1} with a 1% quantum yield at $\lambda \geq 420$ nm.[71] In this nanocomposite, both Pt/TiO_2 and In_2S_3 nanoparticles were in close contact by the embedding of Pt/TiO_2 nanoparticles in the interstices of the In_2S_3. The optimum ratio of In_2S_3 : Pt/TiO_2 was reported to be 3 : 2. Furthermore, Jang *et al.* synthesized a photocatalyst composite from titanium dioxide and $AgGaS_2$ by a solid state reaction followed by a sol–gel method.[74] In the presence of sulfide and sulfite solution, and Pt as a cocatalyst, this composite showed a very good activity for hydrogen under visible light irradiation. Due to the conduction band structure, excited electrons can transfer from $AgGaS_2$ to TiO_2 and from there they can react with protons to produce hydrogen. The maximum quantum yield was 17.5% for the optimum ratio of 1 : 2 (TiO_2 : $AgGaS_2$) and 1% Pt.

Some researchers synthesized nanocomposites of TiO_2 with different carbon-based materials such as carbon-coated metal,[75] carbon quantum dots,[76,77] carbon nanotubes[78] and graphene.[79–82] For example, Peng's group synthesized a novel nanocomposite of carbon coated Ni (denoted as Ni@C) and TiO_2.[75] This nanocomposite consists of nanorods 10 nm in diameter and 40–100 nm in length. By using triethanolamine as a sacrificial reagent, this nanostructure could produce hydrogen under visible light irradiation. The highest activity was obtained when 5% of Ni was used in this nanocomposite (300 μmol h^{-1}). Furthermore, the apparent quantum yields are 12% and 7% for $\lambda > 420$ and $\lambda > 520$ nm, respectively. These yields were much higher than the same for neat Ni@C without TiO_2. Table 1 shows some nanocomposites of titanium dioxide as well as their activity under visible light irradiation.

3.4. CdS-based nanocomposites

CdS is one of the best semiconductors for photocatalytic hydrogen production because of its narrow band gap and conduction band edge position. In other words, it can absorb visible light with long wavelength and also it can reduce protons to hydrogen. However, this photocatalyst has two main disadvantages which are: (1) due to its small band gap, the recombination process of photoexcited electrons and holes is very easy and (2) this semiconductor is unstable under light irradiation and it is effortlessly corroded by excited holes. For these reasons, CdS needs to be combined with other semiconductors in order to overcome its drawbacks.

Due to the high visible light absorption of CdS (2.42 eV), scientists tried to enhance the photocatalytic efficiency of CdS by modifying the nanostructures of this semiconductor. The nanostructure of CdS provided more active sites for the water splitting reaction and so increased its photocatalytic activity.[86] Another technique is preparing CdS in nano-porous structures that can raise the quantum yield up to 60% in the presence of Na_2SO_3 and Na_2S as sacrificial agents ($\lambda \geq 420$ nm).[87] The

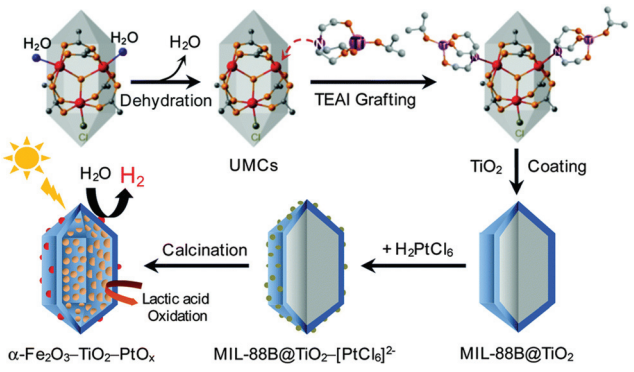

Fig. 8 Schematic illustration of the formation of the hollow Fe_2O_3–TiO_2–PtO_x nanocomposite.[69]

Table 1 Different nanocomposites of TiO_2 active for hydrogen production (λ > 420 nm)

Semiconductor 1	Semiconductor 2	Cocatalyst	Sacrificial reagent	Light source	Hydrogen production (μmol h^{-1} g^{-1})	Quantum yield (%)	Ref.
TiO_2	Carbon-coated Ni (Ni@C)	—	Triethanolamine	300 W Xe, $\lambda \geq 420$ nm	2000	12 at λ = 420 nm 7 at λ = 520 nm	75
TiO_2 nanosheets	Graphene	—	Methanol	350 W Xe	736	No data	79
TiO_2	In_2S_3	Pt	Na_2S–Na_2SO_3	300 W Xe, $\lambda \geq 420$ nm	1350	1 at λ = 420 nm	71
TiO_2 mesocrystals	Au nanoparticles	Pt	Propanol	Xe light, $\lambda > 460$ nm	0.5	No data	83
N,S-doped TiO_2	V_2O_5	Pt	Methanol	125 W Hg, $\lambda \geq 400$ nm	2966	No data	61
TiO_2	MOF MIL-101	Pt	Triethanolamine	450 W Xe, $\lambda \geq 420$ nm	1250	No data	67
TiO_2	MOF MIL-88	PtO_x	Lactic acid	300 W Xe, $\lambda \geq 420$ nm	1100	No data	84
TiO_2	$AgIn_5S_8$	Pt	Na_2S–Na_2SO_3	300 W Xe, $\lambda \geq 420$ nm	850	No data	73
Mesoporous TiO_2	WS_2	Pt	Na_2S	350 W Xe, $\lambda > 430$ nm	200	No data	85
P25	Carbon quantum dot (CQD)	—	Methanol	500 W Halogen, $\lambda > 450$ nm	10	No data	77
$AgGaS_2$	TiO_2	Pt	Na_2S–Na_2SO_3	450 W Hg, $\lambda \geq 420$ nm	4200	17.5 at λ = 420 nm	74
$CaIn_2O_4$	Fe–TiO_2	Pt	KI	300 W Xe, $\lambda \geq 420$ nm	280	No data	63
Graphene	Au–TiO_2	—	Methanol	3W LED, λ = 420 nm	296	4.1 at λ = 420 nm	80
Fe_2O_3	TiO_2	—	Na_2S–Na_2SO_3	300 W Xe, $\lambda \geq 420$ nm	7253	0.94 at λ = 447 nm	64

main reasons for this development in quantum yield are effective charge separation, fast movement of charge carriers, and quick chemical reaction at the interface of the CdS nanostructure. Combing CdS nanoparticles with another semiconductor is another way to enhance its photocatalytic efficiency.[88]

Although metal oxides usually possess wide band gaps and cannot absorb long wavelengths of the sunlight spectrum, they are very stable during photocatalytic processes. Therefore, some studies were done in order to mix these semiconductors together and more efficient photocatalysts were obtained.[55,89–99] For instance, Wang and co-workers prepared core–shell nanostructures from ZnO and CdS.[89] This nanocomposite was able to split water to produce H_2 with sacrificial reagents. Interestingly, loading of a RuO_2 cocatalyst showed greater activity than Pt metal. In addition, the ratio of ZnO to CdS in $(ZnO)_{1-x}(CdS)_x$ strongly affected its photocatalytic efficiency and it dropped slightly by raising the CdS molar ratio. The highest H_2 evolution is 2.96 mmol h^{-1} g^{-1} for x = 0.2, which is 34.4 times and 7.8 times higher than that of ZnO nanorods (prepared by the hydrothermal route) and CdS (prepared by the solid state route), respectively. As mentioned before, RuO_2 has a great impact on the photocatalytic activity, resulting in a sudden increase by around 200%. This nanocomposite could constantly produce H_2 for more than 30 h. Hou *et al.* synthesized a nanocomposite of CdS (2.45 eV) and TaON (2.5 eV) in a core–shell structure.[91] They deposited TaON on the core of CdS and used Pt as a cocatalyst. Due to the band edge positions of these semiconductors, electrons migrate from CdS to TaON and holes can move from TaON to CdS. Although hydrogen evolution rates for pure CdS and TaON were 13.5 and 9 μmol h^{-1}, respectively, this nanocomposite could evolve 306 μmol h^{-1} hydrogen using a sacrificial reagent. Moreover, combining this nanostructure with 1 wt% graphene oxide led to the production of more than two times more hydrogen than the previous one with a 31% quantum yield under visible light irradiation. Nonetheless, they didn't examine the stability of this nanocomposite for multiple cycles in a longer runtime. One of the purposes of combining CdS with other materials is to enhance its stability during the reaction time. Usually the photocatalyst should be run for multiple cycles of hydrogen production in order to observe its stability under light illumination.

In addition to binary metal oxides, some researchers made nanocomposites of CdS and ternary metal oxides.[100–103,110,111] In these nanostructures, generated holes can transfer from CdS to the metal oxides, due to their valence band positions, and photoexcited electrons remain in the conduction band of CdS and reduce protons to hydrogen. These charge carriers' movements are completely different than in other nanocomposites. Usually electrons transfer to other semiconductors from CdS, but in this case holes transfer and so both charge recombination and photocorrosion are avoided. However, it should be noted that the synthesis procedure of these ternary nanocomposites is usually complicated and needs careful attention in order to obtain the desired nanostructure.

Furthermore, CdS can be combined with other metal sulfides in various morphologies such as nanocrystals,[104] nanowires[105] and nano-layers[106] in order to enhance its efficiency. Among all metal sulfides, ZnS attracts more attention due to its strong ability to form a solid solution with CdS which results in higher charge separation and greater quantum efficiency.[107–114] For example, a solid solution of $(Zn_{0.95}Cu_{0.05})_{1-x}Cd_xS$ was examined with various ratios of Cd for H_2 production under visible light and in the presence of SO_3^{2-} and S_2^{2-}.[107] This solid solution consisted of nanocrystals of about 2–5 nm and had a band gap of 2.0 eV. This nanostructure showed 508 μmol h^{-1} hydrogen without any cocatalyst and possessed a quantum yield of 15.7% under visible light when x was equal to 0.33. However, by depositing 0.75% Pt, its activity was enhanced significantly and the hydrogen production and quantum yield reached 1.09 mmol h^{-1} and 31.8%, respectively. Moreover, this nanocomposite was stable after three 12 h cycles. Zhang *et al.* synthesized a nanocrystal of a ZnS–CdS solid solution that was involved in H_2 evolution at 420 nm.[109] They used MoS_2 as a cocatalyst and reported that with 0.2 wt% of this cocatalyst, the hydrogen formation was 36 times higher than for CdS with noble metals as cocatalysts.[115,116] Moreover, Liu *et al.* showed that nano-twin structures of the $Cd_{1-x}Zn_xS$ solid solution could produce hydrogen from water without noble metals. Its apparent quantum yield was reported to be 43% at 425 nm in the presence of sacrificial reagents.[110] Another type of nanocomposite of ZnS and CdS is the physical mixture of their nanoparticles without making a solid solution phase. Shen *et al.* improved the nanocrystals of ZnS/CdS (5–10 nm) with In_2S_3 without any surfactant or supports at room temperature and normal pressure.[104] These microspheres could produce hydrogen from an aqueous solution of sulfide and sulfite ions with no cocatalysts and it was reported that the quantum yield reached 40.9% at $\lambda \geq 420$ nm. The optimum ratio of CdS : ZnS is 75%, which can produce 8.1 mmol h^{-1} g^{-1} hydrogen. Despite the fact that this nanocomposite showed a very high hydrogen evolution, no further experiments were done to examine its stability during hydrogen production, which should be considered in further studies.

In addition to a solid solution, CdS can mix with other metal sulfides in order to increase hydrogen production under visible light irradiation.[105,117–119] For instance, TiS_2 and TaS_2 are both semiconductors with small band gaps less than 1 eV. A nano-layer combination of one of these two semiconductors with nanoparticles of CdS resulted in highly efficient photocatalysts for H_2 evolution from an aqueous solution of benzyl alcohol.[106] The nanocomposite of TiS_2 and CdS could generate 1000 μmol h^{-1} g^{-1} hydrogen, whereas the other one (TaS_2 and CdS) showed 2.3 times higher hydrogen evolution (2320 μmol h^{-1} g^{-1}) under visible light irradiation. The reason for this phenomenon was explained by the metallic nature of few-layer TaS_2. In another study, Zhang *et al.* deposited NiS nanoparticles onto the CdS surface with the help of the hydrothermal route.[117] They reported that the nanocomposite with 1.2% of NiS had the highest activity and quantum yield. Its quantum efficiency under visible light irradiation (λ > 420 nm) was 51.3%, which was the highest photocatalyst activity without a noble metal cocatalyst. In addition, its H_2 evolution rate was 2.18 mmol h^{-1}, which was 35 times higher than that of CdS alone. Hou *et al.* decorated $CdLa_2S_4$ microspheres with CdS nanocrystals by a hydrothermal procedure in order to enhance hydrogen generation.[114] Due to the intimate contact of these nanoparticles and also the high dispersion of CdS nanocrystals, this nanocomposite exhibited a significant quantum yield of 54% under the visible light region corresponding to 2250 μmol h^{-1} g^{-1}, which was 9 times higher than for the pristine $CdLa_2S_4$.

Carbon nanotubes are one of the most famous building blocks for synthesizing nanostructures that can be combined with diverse semiconductors, particularly CdS, in order to enhance the charge separation step, as demonstrated in Fig. 9.[120–125] Furthermore, graphene nanosheets have some special properties such as high surface area, high charge carrier mobility (due to their two-dimensional sp^2-hybridization), and good mechanical stability.[126] The intimate contact between CdS and graphene can enhance the migration of photoexcited electrons and can surpass the recombination process more efficiently. In principle, photoexcited electrons move from the conduction band of the CdS to graphene and in accordance with the great mobility of electrons on the graphene sheets, the recombination process is partially prevented.[123,125,127–133] For instance, Li *et al.* synthesized CdS nanoparticles of about 3 nm diameter in an autoclave and they dispersed them completely onto graphene nanosheets.[133] This nanocomposite, which had 1 wt% graphene and 0.5 wt% Pt, showed 1.12 mmol h^{-1} hydrogen evolution from a solution of lactic acid. This rate of hydrogen production was around 5 times higher than for pristine CdS and the apparent quantum efficiency was reported to be 22.5% at $\lambda \geq 420$ nm.

There have been different methods to synthesize graphene-based photocatalysts, but the simplest and most direct technique is to mix graphene with target semiconductors.[134–136]

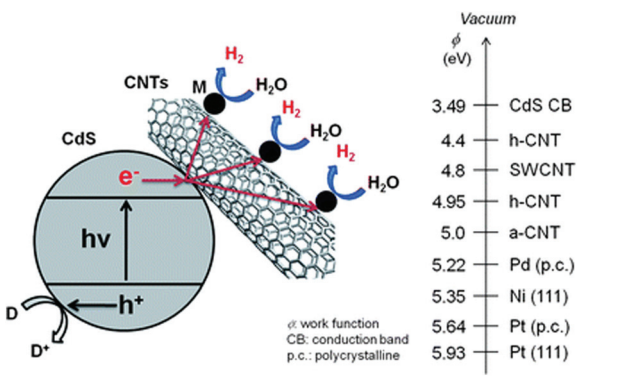

Fig. 9 Illustration of photocatalytic hydrogen production in CdS/CNT/M suspensions under light irradiation. M and D refer to metal catalyst and electron donor, respectively. On the right-hand side, the reported work functions of selected materials are given.[121]

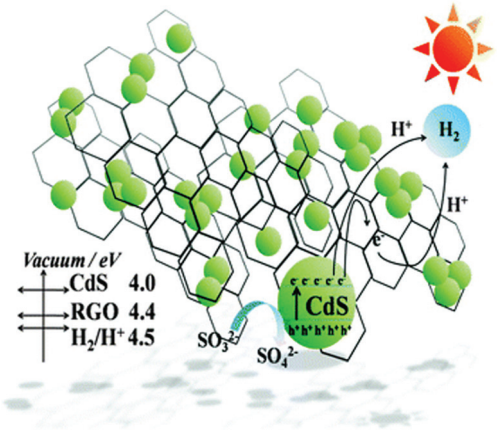

Fig. 10 Schematic diagram of the proposed mechanism for photocatalytic H_2 production over RGO–CdS.[146]

The other popular method to provide nanocomposites of various semiconductors with graphene is an *in situ* growth method in which graphene oxide (GO)[91,133,137] or reduced graphene oxide (RGO)[138–146] is chosen as the starting material.[147] Nanocrystals of CdS or other semiconductors can grow on the surface of graphene nanosheets *via* oxygen-containing functional groups which act as nucleation sites.[148] The structure and electrical properties of RGO as well as the location of the conduction band of CdS and RGO lead the transfer of photoexcited electrons from CdS to RGO and from there they can reduce hydrogen atoms (Fig. 10).

Table 2 summarizes the hydrogen production of different nanocomposites of CdS under visible light irradiation with their quantum yields.

3.5. CdS and TiO_2 nanostructures

TiO_2 and CdS are the most studied semiconductors in recent decades due to their photocatalytic properties and benefits. However, each of them has some drawbacks that limit their applications for hydrogen production from sunlight. For example, TiO_2 has a wide band gap inapplicable for visible light absorption and CdS is unstable during photocatalytic reactions. The combination of these semiconductors at the nanoscale leads to more efficient photocatalysts that can generate hydrogen under visible light irradiation with high stability. Under visible light illumination, CdS can absorb photons and produce holes and electrons. Although TiO_2 cannot absorb visible light, due to its wide band gap, excited electrons can move from CdS to TiO_2. This leads to better charge separation, and results in a higher quantum yield. It should be noted that the excited holes remain in the valence band of CdS and from there they can oxidize any sacrificial agents.[161,162] Various nanocomposites with different morphologies can be created from CdS and TiO_2, as shown in Table 3. Some important morphologies will be discussed here, which result in higher light absorption and higher hydrogen evolution in the visible light region.

Generally, two different morphologies for mixing CdS nanoparticles and titanate nanotubes have been proposed in order to improve photocatalytic activity, as illustrated in Fig. 11.[163–168] CdS/titanate nanotubes (CdS/TNTs) were reported to have a higher increase in photocatalytic activity in comparison to traditional nanocomposite CdS@TNTs.[163] The CdS/TNT nanostructures lead to a proper dispersion of CdS as well as intimate multipoint contacts between two nanocrystals. It is clear that the ratio of Cd : Ti plays an important role in photocatalyst activity. The optimum value of this proportion was 0.05, which corresponds to 6 wt% of CdS in the photocatalysts. With the optimum cocatalyst quantity of Pt (2.0 wt%), the CdS/TNTs could generate 353.4 μmol h^{-1} hydrogen with a 25.5% quantum yield under visible light. Nevertheless, the quantum yield of traditional CdS@TNTs could hardly reach 2.7% and as mentioned before, changing the structure of the nanoparticles can have major impacts on their activity. It is noteworthy that this nanocomposite was stable for hydrogen production during six 120 h cycles. Therefore, this nanostructure noticeably improved the stability of the photocatalyst during hydrogen evolution.

Many researchers have investigated the deposition of CdS nanoparticles inside different nanostructures of titanate, such as tubular and nanotubes, with the aim of obtaining highly efficient nanocomposites.[164,169] Li *et al.* homogeneously deposited CdS nanoparticles inside TiO_2 nanotubes.[164] They examined its photocatalytic water splitting with electron donors containing S^{2-} and SO_3^{2-} at a wavelength of 420 nm. They attained a 43.4% quantum yield for H_2 evolution. This is due to the quantum size effect of CdS nanoparticles as well as synergetic effects between two nanocomposites. This also means that the potential energy at the interface of CdS and TiO_2 would help electrons to transfer from CdS to TiO_2 more easily and consequently enhanced the photocatalytic activity.

CdS nanoparticles can also be deposited on nanosheets of titanate, which leads to increased quantum yield of the nanocomposite.[170–174] The powerful interaction between the titanate 2D nanostructures and CdS helped to create visible light absorption photocatalysts with high stability towards the photocorrosion of CdS. Our group synthesized ultrathin titanate nanodisks (TNDs) by the solvothermal method.[175] After that, we grew both CdS nanoparticles as a visible light semiconductor and Ni nanoparticles as a cocatalyst on the surface of TNDs for hydrogen evolution. This nanocomposite was able to efficiently separate photoexcited charges and as a result it showed a very high activity for water splitting under visible light irradiation. The concept of depositing a cocatalyst on the other surface (here, on TNDs), would help to enhance the photocatalytic activity by increasing charge separation and preventing recombination phenomena. As can be seen in Fig. 12 (a), an excited electron can easily transfer from CdS to the TNDs and from there to the Ni cocatalyst.[170] With an optimum ratio of CdS : TNDs and Ni loading, this nanocomposite can generate H_2 from a water–methanol solution under visible light irradiation. The hydrogen evolution rate was

Table 2 Various nanocomposites of CdS active under visible light illumination

Semiconductor 1	Semiconductor 2	Cocatalyst	Sacrificial reagent	Light source	Hydrogen production ($\mu mol\ h^{-1}\ g^{-1}$)	Quantum yield (%)	Ref.
CdS	SrS	—	Na_2S–Na_2SO_3	300 W Xe, $\lambda > 400$ nm	246	10 at λ = 420 nm	105
CdS	ZnCu	—	Na_2S–Na_2SO_3	300 W Halogen,	1693	15.7 at λ = 420 nm	109
		Pt		$\lambda \geq 420$ nm	3633	31.8 at λ = 420 nm	
CdS	CuIn	—	Na_2S–Na_2SO_3	300 W Xe, $\lambda \geq 420$ nm	649.9	2.14 at λ = 420 nm	108
		Pt			2456	26.5 at λ = 420 nm	
CdS	ZnO	Pt	Na_2S–Na_2SO_3	300 W Xe	2960	No data	89
CdS nanorods	CdSe	Pt	2-Propanol	300 W Xe	40 500	20 at λ = 450 nm	149
CdS	Ni/NiO/$KNbO_3$	—	Isopropanol	500 W Hg–Xe, $\lambda > 400$ nm	203.5	8.8 at $\lambda >$ 400 nm	103
CdS	Ni/NiO/$KNbO_3$	—	Isopropanol	500 W Hg–Xe, $\lambda > 400$ nm	150	4.4 at $\lambda >$ 400 nm	102
CdS	$LaMnO_3$	—	Na_2S–Na_2SO_3	300 W Xe, $\lambda \geq 420$ nm	595	No data	101 and 150
$Cd_{0.8}Zn_{0.2}S$	ZnO	Pt	Benzyl alcohol	450 W Xe	36 500	50.4 at λ = 400 nm	113
CdS nanorods	NiS	—	Na_2S–Na_2SO_3	300 W Xe, $\lambda \geq 420$ nm	1131	6.1 at λ = 420 nm	151
$Cd_{0.1}Zn_{0.9}S$	Multi-walled carbon nanotubes	—	Na_2S–Na_2SO_3	300 W Xe, $\lambda \geq 420$ nm	1563.2	7.9 at λ = 420 nm	122
CdS	CeO_2	—	Na_2S–Na_2SO_3	300 W Xe	223	No data	93
CdS	Multi-walled carbon nanotubes	Pt	Na_2S–Na_2SO_3	300 W Halogen, $\lambda > 400$ nm	825	No data	121
CdS	MWCNTs	—	Na_2S–Na_2SO_3	300 W Xe, $\lambda \geq 420$ nm	4977	2.16 at λ = 420 nm	120
CdS	ZnS	Ru	Formic acid	300 W Xe, $\lambda \geq 420$ nm	6000	20 at λ = 400 nm	152
In_2S_3	CdS–ZnS	—	Na_2S–Na_2SO_3	300 W Xe, $\lambda > 400$ nm	8100	40.9 at λ = 420 nm	104
$CdLa_2S_4$ microspheres	CdS nanocrystals	Pt	Na_2S–Na_2SO_3	300 W Xe, $\lambda \geq 420$ nm	2250	54 at λ = 420 nm	114
ZnS	CdS	—	Na_2S–Na_2SO_3	500 W Halogen	46	No data	112
TaON	CdS	Pt	Na_2S–Na_2SO_3	300 W Xe, $\lambda \geq 420$ nm	1530	15 at λ = 400 nm	91
Graphene oxide	CdS@TaON				3165	31 at λ = 420 nm	
ZnO	CdS	—	Na_2S–Na_2SO_3	500 W Xe, $\lambda > 400$ nm	851	3 at λ = 420 nm	94
$CdOW_4$	CdS	—	Na_2S–Na_2SO_3	500 W Xe	90.25	No data	100
Reduced graphene oxide	CdS	MoS_2	Lactic acid	350 W Xe, $\lambda \geq 420$ nm	1980	9.8 at λ = 420 nm	142
Nanosized MoS_2/graphene hybrid	CdS	MoS_2	Lactic acid	300 W Xe, $\lambda \geq 420$ nm	9000	28.1 at λ = 420 nm	131
Reduced graphene oxide	UiO-66 and CdS	Pt	Na_2S–Na_2SO_3	300 W Xe, $\lambda > 400$ nm	2100	No data	141
Vermiculite	CdS quantum dots		Na_2S–Na_2SO_3	300 W Xe, $\lambda \geq 420$ nm	920	17.7 at λ = 420 nm	153
SiC	CdS particles	Pt	Na_2S–Na_2SO_3	300 W Xe, $\lambda \geq 420$ nm	555	0.2 at λ = 420 nm	154
Framework of structured WO_3	Orderly depositing Au and CdS	—	Na_2S–Na_2SO_3	300 W Xe, $\lambda \geq 420$ nm	1730	No data	95
ZSM-5 type metallosilicates	CdS nanoparticles	—	Na_2S–Na_2SO_3	500 W Osram, $\lambda \geq 420$ nm	11 000	65.62 at λ = 420 nm	155
γ-TaON hollow spheres	CdS nanoparticles	MoS_2	Na_2S–Na_2SO_3	300 W Xe, $\lambda \geq 420$ nm	3142.5	No data	96
ZnO core/shell nanofibers	CdS	—	Na_2S–Na_2SO_3	500 W Xe, $\lambda \geq 420$ nm	354	No data	97

Table 2 *(Contd.)*

Semiconductor 1	Semiconductor 2	Cocatalyst	Sacrificial reagent	Light source	Hydrogen production (μmol h^{-1} g^{-1})	Quantum yield (%)	Ref.
$ZnIn_2S_4$ heterostructures coupled with graphene	CdS quantum dots	Pt	Na_2S–Na_2SO_3	300 W Xe, $\lambda \geq 420$ nm	27 000	56 at λ = 420 nm	132
Carbon nanotubes	$Zn_xCd_{1-x}S$	—	Na_2S–Na_2SO_3	500 W Xe	6030	No data	123
Carbon nanotubes	CdS	NiS	Na_2S–Na_2SO_3	350 W Xe, $\lambda \geq 420$ nm	12 130	No data	124
Reduced graphene oxide	$Cu_{0.02}In_{0.3}ZnS_{1.47}$	Pt	Na_2S–Na_2SO_3	800 W Xe–Hg, $\lambda \geq 420$ nm	3800	No data	140
Ti-MCM-48 mesoporous	CdS	RuO_2	Ethanol	300 W Xe, $\lambda > 400$ nm	2730	36.3 at λ = 400 nm	156
MoO_3	CdS	—	Na_2S–Na_2SO_3	300 W Xe, $\lambda \geq 420$ nm	5250	28.86 at λ = 420 nm	98
Cubic MCM-48 mesoporous	CdS	Pt	Ethanol	300 W Xe, $\lambda > 400$ nm	1810	16.6 at λ = 400 nm	157
Reduced graphene oxide	CdS	—	Na_2S–Na_2SO_3	300 W Xe, $\lambda \geq 420$ nm	4200	10.4 at λ = 420 nm	139
Ga_2O_3	CdS quantum dots	Pt	Lactic acid	300 W Xe, $\lambda \geq 420$ nm	9052	43.6 at λ = 460 nm	99
In_2O_3	CdS		Benzyl alcohol	450 W Xe, $\lambda > 400$ nm	9382	45.3 at λ = 460 nm	106
TiS_2		—			1000	No data	
TaS_2					2320		
MCM-41	CdS	—	Triethanolamine	300 W Xe, $\lambda \geq 430$ nm	47.1	No data	158
$AgGaS_2$	CdS	Pt	Na_2S–Na_2SO_3	450 W Hg, $\lambda \geq 420$ nm	4730	19.7 at λ = 420 nm	159
Reduced graphene oxide	CdS	$Ni(OH)_2$	Na_2S–Na_2SO_3	300 W Xe, $\lambda \geq 420$ nm	4731	No data	138
Graphene oxide	CdS	—	Na_2S–Na_2SO_3	300 W Xe, $\lambda \geq 420$ nm	3410	4.8 at λ = 420 nm	137
Graphene oxide	CdS clusters	Pt	Lactic acid	350 W Xe, $\lambda \geq 420$ nm	5600	22.5 at λ = 420 nm	133
N-graphene	CdS	—	Na_2S–Na_2SO_3	300 W Xe, $\lambda \geq 420$ nm	1050	No data	130
g-C_3N_4	CdS quantum dots	Pt	Methanol	300 W Xe, $\lambda \geq 420$ nm	348	No data	160

15.326 mmol g^{-1} h^{-1} over 15 h of reaction, which results in having a 24% quantum yield at $\lambda \geq 420$ nm. It is noteworthy that this approach of mixing a semiconductor with TNDs can also be used for other efficient visible light active semiconductors. The intimate contact between TNDs and CdS plays a crucial role in this kind of nanostructure. In other words, physical mixing of these semiconductors cannot result in high photocatalytic activity. By growing CdS as well as selectively depositing Ni clusters on the surface of the TNDs by means of an ion exchange method, we were certain that the nanoparticles had intimate contact and so charge carriers can easily transfer between the semiconductors, as shown in Fig. 12(b).[176] In another technique, researchers tried to deposit TiO_2 nanoparticles on CdS nanostructures.[161,162,182–184,186] In most of them, a cocatalyst had to be utilized in order to show hydrogen production. For instance, Jang *et al.* made a nanocomposite of CdS nanowires (NWs) with a high crystallinity, which had TiO_2 nanocrystals on their surfaces, as shown in Fig. 13.[183] Under visible light, this nanostructure displayed hydrogen production from an aqueous solution of sulfide and sulfite ions. The optimum ratio of TiO_2 : CdS in this nanostructure would be 0.2, which led to the highest activity under visible light irradiation. The possible role of TiO_2 NPs is to provide sites for collecting the photoelectrons generated from the CdS NWs, thereby enabling an efficient electron–hole separation as depicted in Fig. 13.

Preparing a nanocomposite is a very delicate process and each step should be considered precisely, even though the nanostructure and crystallinity may change by the order of adding precursors. Park *et al.* showed that reversing the chemical precipitation order of CdS on TiO_2 nanoparticles caused different H_2 evolution rates under the same conditions.[177] They prepared CdS_R by adding Cd^{2+} in an aqueous solution containing S^{2-} and Pt-loaded TiO_2. Another nanocomposite with an equal molar ratio was prepared by adding sulfide drops into the solution of Cd^{2+} and Pt–TiO_2 (Cd_RS). Surprisingly, CdS_R showed 10 times higher hydrogen evolution than Cd_RS under visible light irradiation (Fig. 14).

Khatamian *et al.* prepared a metallosilicate-based (ferrisilicate and aluminosilicate) nanocomposite of CdS/TiO_2 *via* a hydrothermal method.[178] Utilizing a metallosilicate support has many advantages such as offering high surface area and providing a homogeneous dispersion of CdS nanoparticles. Moreover, this support both prevents agglomeration of the

Table 3 Different nanocomposites of CdS and TiO_2

Semiconductor 1	Semiconductor 2	Cocatalyst	Sacrificial reagent	Light source	Hydrogen production ($\mu mol\ h^{-1}\ g^{-1}$)	Quantum yield (%)	Ref.
$Na_2Ti_2O_4(OH)_2$ nanotubes	CdS	Pt	Na_2S–Na_2SO_3	350 W Xe, $\lambda \geq 430$ nm	545	2.7 at λ = 430 nm	167
TiO_2 nanotubes	CdS	Pt	Na_2S–Na_2SO_3	300 W Xe, $\lambda \geq 420$ nm	2680	43.3 at λ = 420 nm	164
Titanate nanotubes	CdS	Pt	Na_2S–Na_2SO_3	500 W Xe, $\lambda \geq 430$ nm	1767	25.5 at λ = 420 nm	163
Titanate nanodisks	CdS	Ni	Ethanol	300 W Xe, $\lambda \geq 420$ nm	11 038	21 at λ = 420 nm	175
Titanate nanodisks	CdS	Ni	Ethanol	300 W Xe, $\lambda \geq 420$ nm	15 326	24 at λ = 420 nm	170
TiO_2 nanosheets	CdS nanoparticles	—	Na_2S–Na_2SO_3	350 W Xe, $\lambda \geq 400$ nm	1651	8.9 at λ = 420 nm	171
TiO_2	CdS	Pt	Na_2S–Na_2SO_3	450 W Xe, $\lambda \geq 420$ nm	4848	No data	177
TiO_2	Hexagonal CdS	—	Na_2S–Na_2SO_3	500 W Osram	8990	No data	178
TiO_2 nanorods	CdS nanoparticles	Ni	Ethanol	300 W Xe, $\lambda \geq 420$ nm	33.63	No data	168
Titanate nanotubes	$Cd_{0.5}Zn_{0.5}S$	—	Na_2S–Na_2SO_3	500 W Xe, $\lambda \geq 430$ nm	1738.5	38.1 at λ = 420 nm	179
TiO_2 nanosheets	CdS NPs	Pt	Lactic acid	350 W Xe, $\lambda \geq 420$ nm	6625	13.9 at λ = 420 nm	172
TiO_2	CdS	Pt	Na_2S–Na_2SO_3	350 W Xe, $\lambda \geq 420$ nm	6720	4.5 at λ = 420 nm	180
Titanate spheres	CdS nanoparticles	—	Na_2S–Na_2SO_3	300 W Xe, $\lambda \geq 420$ nm	75	No data	181
Sub-nanometer-thick layered titanate nanosheets	CdS quantum dots (QDs)	—	Na_2S–Na_2SO_3	300 W Xe, $\lambda \geq 420$ nm	1000	No data	173
Bulk CdS	TiO_2 nanoparticles	Pt	Na_2S–Na_2SO_3	350 W Xe, $\lambda \geq 420$ nm	6400	No data	161
Hex-CdS	TiO_2	Pt	Glycerol	300 W Xe, $\lambda \geq 420$ nm	22	No data	182
TiO_2	CdS				65		
CdS nanowires	TiO_2 nanoparticles	Pt	Na_2S–Na_2SO_3	500 W Xe, $\lambda \geq 420$ nm	110	No data	183
CdS bulk	TiO_2 nanoparticles	Pt	Na_2S–Na_2SO_3	350 W Xe, $\lambda \geq 420$ nm	4224	No data	184
Chromosilicate	CdS–TiO_2	—	Na_2S–Na_2SO_3	500 W Osram, $\lambda \geq 420$ nm	2580	76.27 at λ = 450 nm	185
TiO_2	CdS	Au	Na_2S–Na_2SO_3	300 W Xe, $\lambda \geq 420$ nm	1970	No data	186

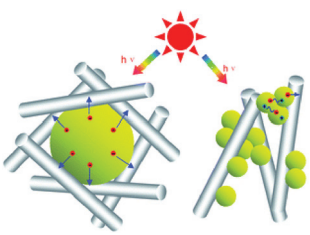

Fig. 11 Schematic illustration of the two different architectures in CdS/TNTs (left) and CdS@TNTs (right).[163]

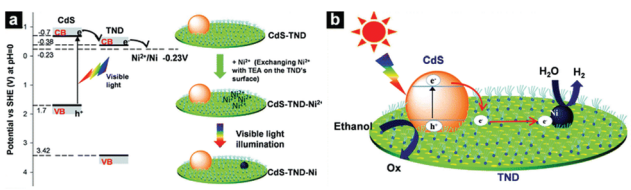

Fig. 12 Schematic illustration of the electron transfer in the photoreduction of Ni^{2+} adsorbed onto the surface of TNDs under visible light illumination and schematic illustration of the formation of Ni clusters on the surface of TNDs by CdS-TND composites by visible light illumination (a). Schematic illustration of the charge transfer in CdS-TND-Ni NPs in the photocatalytic H_2 production from water–ethanol solution under visible light (b).[170]

semiconductor and facilitates electron transfer and separation. It is noteworthy to consider that in applying ferrisilicate, the presence of partially occupied d orbitals of Fe^{3+}, which can interact with TiO_2 orbitals, enhances the photocatalytic activity, while applying aluminosilicate as a support didn't improve its activity compared to the unsupported composite. In the case of the CdS phase, the hexagonal structure showed around a sixfold higher photocatalytic activity than the cubic one.

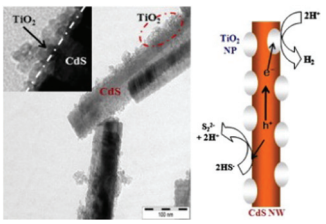

Fig. 13 A nanocomposite consisting of CdS NWs with high crystallinity decorated with nanosized TiO_2 NPs.[183] Image reproduced with permission from Elsevier.

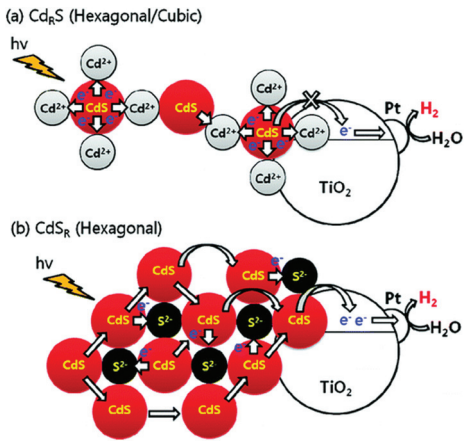

Fig. 14 Schematic illustration of the photocatalytic hydrogen production mechanisms of Cd_RS and CdS_R hybrids.[177]

Vu *et al.* provided a nanocomposite of TiO_2 nanorods and CdS nanoparticles with Ni clusters in order to enhance charge separation and photocatalytic activity.[168] A dominant feature of this nanorod-based material is that nanoparticles of second semiconductors could be dispersed uniformly on the nanorod surface. Ni nanoparticles acting as cocatalysts were selectively deposited on the surfaces of these nanorods. This configuration can improve the efficiency of electron transfer from the sensitized CdS nanoparticles to TiO_2 and then to Ni clusters, as depicted in Fig. 15. The H_2 production rate was 33.36 μmol h^{-1} g^{-1} under visible light in the presence of a sacrificial reagent, which was about 44 times higher than for the neat Ni–CdS system.

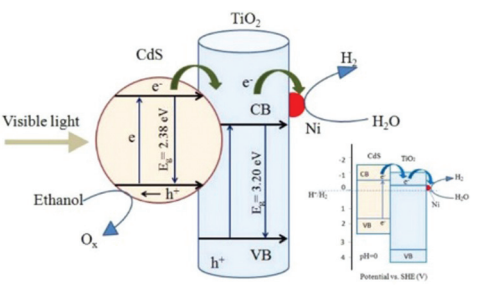

Fig. 15 Mechanistic illustration of the activity of Ni–TiO_2/CdS under visible light for the production of H_2; inset is the potential redox energy corresponding to CdS, TiO_2, and H^+/H_2.[168] Reprinted with permission from ref. 168. Copyright 2015 American Chemical Society.

A new ternary nanostructure of three different nanoparticles was synthesized in order to enhance H_2 production under visible light irradiation.[186] Firstly, they synthesized nanoparticles of Au with an average size of 40 nm. After this step, they grew TiO_2 nanocrystals as a shell structure on the Au nanoparticles *via* a hydrothermal method according to previous research.[187] They then deposited CdS nanoparticles onto the surface of Au@TiO_2 core–shell nanostructures. This ternary nanocomposite showed considerably high activity for H_2 evolution compared to both binary nanostructures (CdS–TiO_2 or Au@TiO_2). This ternary design builds up a transfer path for the photoexcited electrons from CdS to the core Au particles *via* the TiO_2 nanocrystal bridge and thus effectively suppresses the electron–hole recombination on the CdS photocatalyst. However, this nanocomposite is very complicated to obtain and needs precise conditions for each step of the synthesis, which is one of its drawbacks in comparison with other binary nanocomposites for hydrogen production.

3.6. g-C_3N_4-based nanocomposites

Graphitic carbon nitride (g-C_3N_4) is a metal-free semiconductor that consists of *s*-triazine or tri-*s*-triazine units. These units are connected in a two-dimensional graphite-like framework by amino groups in each layer and weak van der Waals forces between layers.[188] As a result, this polymeric semiconductor shows very high thermal and chemical stability. In 2009, Wang *et al.* synthesized g-C_3N_4 from cyanamide by pyrolysis at high temperature (400–600 °C).[189] The obtained semiconductor could not only produce hydrogen under visible light irradiation from an aqueous solution of triethanolamine (TEA), but it also gave a steady hydrogen production rate over 75 h. Since then, other researchers tried to synthesize g-C_3N_4 from other nitrogen-rich precursors such as dicyanamide, urea and melamine.[190] In addition, some other scientists combined it with other semiconductors or charge carrier mediator to boost its photocatalyst activity.[191–196] Here, we discuss various heterojunctions of g-C_3N_4 and semiconductors that could improve hydrogen production under visible light (Table 4).

Due to the structural similarity between carbon bonds in carbon-based nanostructures (nanotubes and graphene) and graphite carbon nitride, it is believed that these materials can mix together and as a result the photocatalytic efficiency will increase substantially.[194,196] For instance, g-C_3N_4 nanosheets were mixed with graphene in order to increase the visible light photocatalytic activity for H_2 generation.[194] This metal-free nanocomposite could generate hydrogen from an aqueous solution of methanol under light illumination (λ > 400 nm). Using 1 wt% of graphene with Pt-loaded g-C_3N_4, the H_2 evolution rate was noticeably enhanced from 147 μmol h^{-1} g^{-1} to 451 μmol h^{-1} g^{-1}. Another group tried to modify g-C_3N_4 by introducing carbon nanotubes into its structure.[196] Despite the fact that the new composite and pure g-C_3N_4 are very similar in their properties, the new photocatalyst possessed higher activity (around 2.5 times) than the other one. With

Table 4 Different nanocomposites of graphitic carbon nitride

Semiconductor 1	Semiconductor 2	Cocatalyst	Sacrificial reagent	Light source	Hydrogen production (μmol h^{-1} g^{-1})	Quantum yield (%)	Ref.
Layered g-C_3N_4 sheets	Graphitized polyacrylonitrile	Pt	Triethanolamine	150 W Halogen, $\lambda \geq 420$ nm	370	No data	203
g-C_3N_4	Nickel sulfide (NiS)	—	Triethanolamine	300 W Xe, $\lambda \geq 420$ nm	447.7	No data	197
g-C_3N_4	Zinc phthalocyanine	Pt	Ascorbic acid	350 W Xe, $\lambda \geq 420$ nm	12 500	1.85 at λ = 700 nm	204
g-C_3N_4	C/N co-doped TiO2	Ag	Methanol	300 W Xe, $\lambda \geq 420$ nm	96	No data	198
g-C_3N_4	PEDOT	Pt	Triethanolamine	300 W Xe, $\lambda \geq 420$ nm	327	No data	195
g-C_3N_4	WO_3	Pt	Triethanolamine	300 W Xe, $\lambda \geq 420$ nm	110	0.9 at λ = 420 nm	199
g-C_3N_4	Carbon nanotubes	Pt	Triethanolamine	350 W Xe, $\lambda \geq 420$ nm	394	No data	196
g-C_3N_4	$ZnFe_2O_4$	Pt	Triethanolamine	300 W Xe, $\lambda \geq 420$ nm	200.77	No data	200
g-C_3N_4	Ag_2S	—	Methanol	300 W Xe, $\lambda \geq 420$ nm	200	No data	201
g-C_3N_4	TiO_2	Pt	Triethanolamine	300 W Xe, $\lambda \geq 420$ nm	1780	No data	192
g-C_3N_4	Poly(3-hexylthiophene)	Pt	Na_2S–Na_2SO_3	300 W Hg, $\lambda \geq 420$ nm	1866	2.9 at λ = 420 nm	205
g-C_3N_4	Au nanoparticles	—	Triethanolamine	300 W Xe, $\lambda \geq 420$ nm	8870	No data	206
C_3N_4	NiS	—	Triethanolamine	300 W Xe, $\lambda \geq 420$ nm	482	1.99 at λ = 440 nm	207
Carbon nitride	N-doped tantalic acid	—	Methanol	300 W Xe, $\lambda \geq 420$ nm	70.6	4.89 at λ = 420 nm	208
g-C_3N_4	$SrTiO_3$: Rh	Pt	Methanol	300 W Xe, $\lambda \geq 420$ nm	2223	5.59 at λ = 420 nm	193
g-C_3N_4	MWNTs	Pt	Methanol	350 W Xe, $\lambda \geq 420$ nm	75.8	No data	202

optimal amounts of carbon nanotubes (2 wt%), it produced 394 μmol h^{-1} g^{-1} hydrogen under visible light illumination because of the increased lifetime of excited electron and holes and the prevention of their recombination.

Furthermore, other semiconductors can be combined with g-C_3N_4 in order to prevent charge recombination.[192,193,197–202] For example, Chai *et al.* generated a nanocomposite consisting of porous g-C_3N_4 with TiO_2 nanoparticles.[192] In accordance with the close interaction between these nanomaterials, when this nanocomposite was improved using Pt metal as a cocatalyst, it showed hydrogen evolution under visible light illumination (λ > 420 nm). The maximum hydrogen evolution (178 μmol h^{-1}) was achieved when the mass ratio of g-C_3N_4 and TiO_2 was 70 to 30. Kang *et al.* synthesized a composite of graphitic carbon nitride and Rh-doped $SrTiO_3$.[193] Using Pt as a cocatalyst, this photocatalyst could produce hydrogen from an aqueous solution of methanol at 410 nm with a quantum yield of 5.5%. Doping Rh into the structure of $SrTiO_3$ provides a donor level in the band gap region of $SrTiO_3$: Rh. As a result, the excited holes can easily transfer from the $SrTiO_3$: Rh semiconductor to the carbon nitride and the excited electrons move from the conduction band of the g-C_3N_4 to the $SrTiO_3$: Rh. This leads to high charge separation and higher hydrogen production (2223 μmol h^{-1} g^{-1}) in comparison to each of the semiconductors alone.

3.7. Other nanocomposites

In spite of the above nanocomposites and nanostructures, scientists have tried to synthesize and combine other nanoscale semiconductors in order to achieve highly efficient photocatalysts for hydrogen evolution under visible light illumination. 1D and 2D nanoparticles and nanostructures such as nanowires, nanotubes, nanorods, nanobelts, nanosheets, and nanoplates, have interested researchers in the last decade for water splitting *via* sunlight.[209–222] The combination of these kinds of nanostructures can effectively enhance charge separation and prevent the recombination process, and so increase the photocatalyst efficiency as summarized in Table 5.

Andrew Frame *et al.* found that CdSe nanoribbons were active in photocatalytic H_2 evolution from a S^{2-}/SO_3^{2-} solution under visible light, whereas bulk CdSe was not.[217] By linking these nanoparticles with MoS_2 nanoplates, the activity was enhanced by about four times and so their quantum yields reached 9.2% at 440 nm. Interestingly, in this nanocomposite Pt cannot be used as a cocatalyst due to sulfide poisoning of the surface sites.

Jing *et al.* synthesized a Cu-doped core–shell tubular nanocomposite of ZnO/ZnS.[218] They tried to deposit Cu-doped ZnS nanoparticles on the outside of ZnO nanotubes. As a result, this nanocomposite showed higher hydrogen evolution than

Table 5 Other nanocomposites for hydrogen production under visible light irradiation

Semiconductor 1	Semiconductor 2	Cocatalyst	Sacrificial reagent	Light source	Hydrogen production (μmol h^{-1} g^{-1})	Quantum yield (%)	Ref.
ZnS	ZnO core–shell nanotubes	Pt	Na_2S–Na_2SO_3	300 W Xe, $\lambda \geq 420$ nm	18	No data	218
$NaNbO_3$ nanorods	In_2O_3 nanoparticles	Pt	Methanol	300 W Xe, $\lambda \geq 420$ nm	16.4	1.45 at λ = 420 nm	219
$MgFe_2O_4$	$CaFe_2O_4$	RuO_2 on guest and Pt on host	Methanol	450 W W-Arc, $\lambda \geq 420$ nm	82.1	10.1 at λ = 420 nm	220
Al_2O_3–MCM-41	Fe	—	Methanol	150 W Hg, $\lambda \geq 400$ nm	1460	6.1 at λ = 400 nm	221
Fe_2O_3	Fe_4N	—	—	300 W Xe, $\lambda \geq 420$ nm	25	1.7 at λ = 400 nm	222
WO_3	Au	Pt	Glycerol	300 W Xe, $\lambda \geq 420$ nm	132	0.2 at λ = 420 nm	223
Ta_2O_5	Au	Pt	Methanol	350 W Xe, $\lambda \geq 420$ nm	55	No data	224
Ta_3N_5					150		
ZnS–Bi_2S_3 nanorods	ZnO	—	Glycerol	300 W Xe, $\lambda \geq 420$ nm	310	No data	225
Rh-doped $SrTiO_3$	$BiVO_4$	Ru	—	350 W Xe, $\lambda \geq 420$ nm	200	1.6 at λ = 400 nm	226
ZnO	In_2O_3	—	Methanol	300 W Xe, $\lambda \geq 420$ nm	1784	No data	227
$SrTiO_3$ (La,Cr)	Sr_2TiO_4	Pt	Methanol	300 W Xe, $\lambda \geq 420$ nm	24	No data	228
Bi-$NaTaO_3$	Bi_2O_3	—	Methanol	300 W Xe, $\lambda \geq 420$ nm	102.5	No data	229
$GdCrO_3$	$Gd_2Ti_2O_7$	—	Methanol	350 W Hg, $\lambda \geq 400$ nm	1231.5	4.1 at λ = 400 nm	230
$Ag_3PW_{12}O_{40}$	Carbon quantum dots	Ag	—	300 W Xe, $\lambda \geq 420$ nm	3.8	4.9 at λ = 480 nm	231
$Cu_{1.8}S$	ZnS	—	Na_2S–Na_2SO_3	300 W Xe, $\lambda \geq 420$ nm	467	No data	232
2D ultrathin curled $ZnIn_2S_4$ nanosheets	MoS_2	—	Na_2S–Na_2SO_3	300 W Xe, $\lambda \geq 420$ nm	975	No data	233
In_2O_3	$Gd_2Ti_2O_7$	—	Methanol	300 W Xe, $\lambda \geq 420$ nm	5789	No data	234
$K_2La_2Ti_3O_{10}$	$ZnIn_2S_4$	—	Na_2S–Na_2SO_3	300 W Xe, $\lambda \geq 420$ nm	2096	No data	235
Ta_2O_5	In_2O_3	Pt	Methanol	300 W Xe, $\lambda \geq 420$ nm	10	No data	236

the undoped ZnO/ZnS nanocomposite. Copper ions act as the donor level to induce the visible light response of ZnS and thus excited electrons can migrate from ZnS to ZnO and from there they reduce protons.

Two ferrites of calcium (CFO) and magnesium (MFO), *i.e.* $CaFe_2O_4$ and $MgFe_2O_4$ were used to synthesize nanocomposites for the H_2 evolution reaction.[220] Due to the difference in band position of these semiconductors, photoexcited electrons transfer from $CaFe_2O_4$ to $MgFe_2O_4$, whereas the holes can move *vice versa*. Both CFO and MFO are active for hydrogen production under visible light irradiation when promoted with cocatalysts (Pt and RuO_2 for CFO and MFO, respectively). However, the nanocomposite of CFO and MFO produced 82.8 mmol h^{-1} g^{-1} with a quantum yield of 10.1% which was an order of magnitude higher than that of RuO_2/MFO or Pt/CFO.

Pradhan *et al.* synthesized a mesoporous nanocomposite of Fe/Al_2O_3–MCM-41 with a pore size of 50 nm. They reported that this photocatalyst with 5 wt% of Fe showed hydrogen production activity under visible light (146 μmol h^{-1}) with a quantum yield of 6.1%. The main reason for such activity is due to the properties of mesoporous materials, which are their high pore volume, narrow pore size distribution and high surface area. Furthermore, iron doping on the surface helped to absorb visible light, although the mesoporous nanocomposite by itself didn't show any activity for $\lambda > 400$ nm.[221]

4. Conclusion

Photocatalytic hydrogen production based on solar-driven water splitting is one of the best ways to use solar energy. However, industrial application of this strategy is still hindered by its currently low efficiency originating from the lack of efficient photocatalysts. Various methods have been developed to boost the photocatalyst efficiency such as metal or non-metal doping of wide band-gap semiconductors to decrease their band gap and applying cocatalysts to improve the charge

separation and to provide active sites on the surface of the semiconductor for water splitting. Making multicomponent heterojunctions of different semiconductor nanocomposites offers an effective tool to extend sunlight absorption and also to increase charge carrier lifetimes by enhancing charge separation. Nanostructured photocatalysts can improve the efficiency by providing a large surface area and small particle size. As a result, charge carriers transfer noticeably small distances from the bulk material to its surface , which partially limits the recombination phenomenon.

Among various semiconductor heterojunctions for photocatalytic hydrogen generation, TiO_2- and CdS-based systems have been most studied. TiO_2 is one of the applicable and commercial photocatalysts that can be utilized in different photocatalysis processes. Combining nano-sized TiO_2 with suitable small band-gap semiconductors produces nanocomposite photocatalysts which exhibit an improvement in hydrogen production from the visible light region. CdS, on the other hand, has been widely studied for hydrogen production because of its relatively small band gap and suitable electronic band structure. Combining CdS with other semiconductors helps to improve the charge separation and stability of CdS which leads to the formation of efficient nanocomposites for hydrogen generation. Currently, CdS-based photocatalysts are among the best photocatalysts for hydrogen generation under visible light.

Although coupling semiconductors has been shown to improve the photocatalytic efficiency of the photocatalyst, the overall efficiency for hydrogen production using sunlight is still very low. Factors such as composition, interface between the semiconductors, and morphology of each component, all of which determine the photocatalytic activity of such materials, need to be further elucidated in great detail. Furthermore, the charge transfer in multi-component photocatalysts is sensitively and greatly affected by how the hybrid is organized. Thus, the relative position of both the semiconductor and cocatalysts needs to be controlled in order to optimize the electron transfer throughout the photocatalyst. Besides this, new material design and innovative strategies for improving the charge separation and sunlight absorption of the photocatalysts are also very important for the realization of hydrogen production based on solar driven water splitting.

Notes and references

1 N. S. Lewis and D. G. Nocera, *Proc. Natl. Acad. Sci. U. S. A.*, 2006, **103**, 15729–15735.
2 W. Fan, Q. Zhang and Y. Wang, *Phys. Chem. Chem. Phys.*, 2013, **15**, 2632–2649.
3 A. Fujishima, *Nature*, 1972, **238**, 37–38.
4 A. J. Bard, *J. Photochem.*, 1979, **10**, 59–75.
5 B. D. Alexander, P. J. Kulesza, I. Rutkowska, R. Solarska and J. Augustynski, *J. Mater. Chem.*, 2008, **18**, 2298–2303.
6 T. Bak, J. Nowotny, M. Rekas and C. Sorrell, *Int. J. Hydrogen Energy*, 2002, **27**, 991–1022.
7 A. Kudo and Y. Miseki, *Chem. Soc. Rev.*, 2009, **38**, 253–278.
8 D. Zhang, G. Li, H. Li and Y. Lu, *Chem. – Asian J.*, 2013, **8**, 26–40.
9 Y. Sang, H. Liu and A. Umar, *ChemCatChem*, 2015, **7**, 559–573.
10 Y. Tang, W. Di, X. Zhai, R. Yang and W. Qin, *ACS Catal.*, 2013, **3**, 405–412.
11 S. Shen, J. Shi, P. Guo and L. Guo, *Int. J. Nanotechnol.*, 2011, **8**, 523–591.
12 J. Nowotny, C. Sorrell, T. Bak and L. Sheppard, *Sol. Energy*, 2005, **78**, 593–602.
13 Z. Zou, J. Ye, K. Sayama and H. Arakawa, *Nature*, 2001, **414**, 625–627.
14 X. Chen, S. Shen, L. Guo and S. S. Mao, *Chem. Rev.*, 2010, **110**, 6503–6570.
15 K. Maeda, K. Teramura and K. Domen, *J. Catal.*, 2008, **254**, 198–204.
16 A. J. Esswein and D. G. Nocera, *Chem. Rev.*, 2007, **107**, 4022–4047.
17 A. Galińska and J. Walendziewski, *Energy Fuels*, 2005, **19**, 1143–1147.
18 J. Wang, P. Yang, B. Cao, J. Zhao and Z. Zhu, *Appl. Surf. Sci.*, 2015, **325**, 86–90.
19 F. Guzman, S. S. C. Chuang and C. Yang, *Ind. Eng. Chem. Res.*, 2012, **52**, 61–65.
20 T. Kawai and T. Sakata, *J. Chem. Soc., Chem. Commun.*, 1979, 1047–1048.
21 T. Kawai and T. Sakata, *J. Chem. Soc., Chem. Commun.*, 1980, 694–695.
22 P. Zhou, J. Yu and M. Jaroniec, *Adv. Mater.*, 2014, **26**, 4920–4935.
23 X. Zong, G. Lu and L. Wang, *Nanocatal. Synth. Appl.*, 2013, 495–559.
24 P. Zhou, J. Yu and M. Jaroniec, *Adv. Mater.*, 2014, **26**, 4920–4935.
25 K. Maeda, *ACS Catal.*, 2013, **3**, 1486–1503.
26 K. Sayama, K. Mukasa, R. Abe, Y. Abe and H. Arakawa, *J. Photochem. Photobiol., A*, 2002, **148**, 71–77.
27 N. Serpone, G. Sauve, R. Koch, H. Tahiri, P. Pichat, P. Piccinini, E. Pelizzetti and H. Hidaka, *J. Photochem. Photobiol., A*, 1996, **94**, 191–203.
28 S. Khan and S. Majumder, *Int. J. Hydrogen Energy*, 1989, **14**, 653–660.
29 J. Akikusa and S. U. Khan, *Int. J. Hydrogen Energy*, 2002, **27**, 863–870.
30 K. Gurunathan, *Int. J. Hydrogen Energy*, 2004, **29**, 933–940.
31 J. S. Jang, K. Y. Yoon, X. Xiao, F.-R. F. Fan and A. J. Bard, *Chem. Mater.*, 2009, **21**, 4803–4810.
32 J. S. Jang, S. H. Choi, H. G. Kim and J. S. Lee, *J. Phys. Chem. C*, 2008, **112**, 17200–17205.
33 K. Maeda, K. Teramura, D. Lu, N. Saito, Y. Inoue and K. Domen, *Angew. Chem., Int. Ed.*, 2006, **118**, 7970–7973.
34 K. Domen, S. Naito, T. Onishi and K. Tamaru, *Chem. Phys. Lett.*, 1982, **92**, 433–434.
35 S. Sato and J. White, *Chem. Phys. Lett.*, 1980, **72**, 83–86.

36 J. Lehn, J. Sauvage, R. Zlessel and L. Hilaire, *Isr. J. Chem.*, 1982, **22**, 168–172.
37 K. Yamaguti and S. Sato, *J. Chem. Soc., Faraday Trans. 1*, 1985, **81**, 1237–1246.
38 A. Iwase, H. Kato and A. Kudo, *Catal. Lett.*, 2006, **108**, 7–10.
39 Y. Inoue, O. Hayashi and K. Sato, *J. Chem. Soc., Faraday Trans.*, 1990, **86**, 2277–2282.
40 K. Maeda, K. Teramura, N. Saito, Y. Inoue and K. Domen, *J. Catal.*, 2006, **243**, 303–308.
41 H. Sheng, L. Yu, Y. Jian-Hua and Y. Ying, in *Nanotechnology for Sustainable Energy*, American Chemical Society, 2013, ch. 9, vol. 1140, pp. 219–241.
42 R. Marschall, *Adv. Funct. Mater.*, 2014, **24**, 2421–2440.
43 A. L. Linsebigler, G. Lu and J. T. Yates Jr., *Chem. Rev.*, 1995, **95**, 735–758.
44 M. Sathish, B. Viswanathan and R. Viswanath, *Int. J. Hydrogen Energy*, 2006, **31**, 891–898.
45 P. S. Lunawat, R. Kumar and N. M. Gupta, *Catal. Lett.*, 2008, **121**, 226–233.
46 K. Parida, K. Reddy, S. Martha, D. Das and N. Biswal, *Int. J. Hydrogen Energy*, 2010, **35**, 12161–12168.
47 L. Yuliati, J.-H. Yang, X. Wang, K. Maeda, T. Takata, M. Antonietti and K. Domen, *J. Mater. Chem.*, 2010, **20**, 4295–4298.
48 Z. Zhang, C.-C. Wang, R. Zakaria and J. Y. Ying, *J. Phys. Chem. B*, 1998, **102**, 10871–10878.
49 N. Serpone, D. Lawless, R. Khairutdinov and E. Pelizzetti, *J. Phys. Chem.*, 1995, **99**, 16655–16661.
50 T. Ishihara, N. S. Baik, N. Ono, H. Nishiguchi and Y. Takita, *J. Photochem. Photobiol., A*, 2004, **167**, 149–157.
51 N. Bao, L. Shen, T. Takata, K. Domen, A. Gupta, K. Yanagisawa and C. A. Grimes, *J. Phys. Chem. C*, 2007, **111**, 17527–17534.
52 I. Gur, N. A. Fromer, M. L. Geier and A. P. Alivisatos, *Science*, 2005, **310**, 462–465.
53 J. S. Steckel, J. P. Zimmer, S. Coe-Sullivan, N. E. Stott, V. Bulović and M. G. Bawendi, *Angew. Chem., Int. Ed.*, 2004, **43**, 2154–2158.
54 Y. Ohko, T. Tatsuma, T. Fujii, K. Naoi, C. Niwa, Y. Kubota and A. Fujishima, *Nat. Mater.*, 2003, **2**, 29–31.
55 X. Wang, G. Liu, L. Wang, Z. G. Chen, G. Q. M. Lu and H. M. Cheng, *Adv. Energy Mater.*, 2012, **2**, 42–46.
56 J. Zhu and M. Zäch, *Curr. Opin. Colloid Interface Sci.*, 2009, **14**, 260–269.
57 S.-D. Mo and W. Ching, *Phys. Rev. B: Condens. Matter*, 1995, **51**, 13023.
58 Y. Liu, L. Guo, W. Yan and H. Liu, *J. Power Sources*, 2006, **159**, 1300–1304.
59 H. Yang, L. Guo, W. Yan and H. Liu, *J. Power Sources*, 2006, **159**, 1305–1309.
60 B. Naik, S. Martha and K. Parida, *Int. J. Hydrogen Energy*, 2011, **36**, 2794–2802.
61 S. Martha, D. P. Das, N. Biswal and K. M. Parida, *J. Mater. Chem.*, 2012, **22**, 10695–10703.
62 M. Xie, Y. Feng, Y. Luan, X. Fu and L. Jing, *ChemPlusChem*, 2014, **79**, 737–742.
63 W. Yan, Y. Zhang, W. Xie, S. Sun, J. Ding, J. Bao and C. Gao, *J. Phys. Chem. C*, 2014, **118**, 6077–6083.
64 S. Zhu, F. Yao, C. Yin, Y. Li, W. Peng, J. Ma and D. Zhang, *Microporous Mesoporous Mater.*, 2014, **190**, 10–16.
65 M. Xie, X. Fu, L. Jing, P. Luan, Y. Feng and H. Fu, *Adv. Energy Mater.*, 2014, **4**, 1300995–1301001.
66 Y. H. Ng, A. Iwase, A. Kudo and R. Amal, *J. Phys. Chem. Lett.*, 2010, **1**, 2607–2612.
67 K. E. deKrafft, C. Wang and W. Lin, *Adv. Mater.*, 2012, **24**, 2014–2018.
68 E. Thimsen, S. Biswas, C. S. Lo and P. Biswas, *J. Phys. Chem. C*, 2009, **113**, 2014–2021.
69 M.-H. Pham, T. C. Dinh, G.-T. Vuong, N.-D. Ta and T.-O. Do, *Phys. Chem. Chem. Phys.*, 2014, **16**, 5937–5941.
70 S. K. Sarkar, J. Y. Kim, D. N. Goldstein, N. R. Neale, K. Zhu, C. M. Elliott, A. J. Frank and S. M. George, *J. Phys. Chem. C*, 2010, **114**, 8032–8039.
71 B. Chai, T. Peng, P. Zeng and J. Mao, *J. Mater. Chem.*, 2011, **21**, 14587–14593.
72 S. Shen and L. Guo, *J. Solid State Chem.*, 2006, **179**, 2629–2635.
73 K. Li, B. Chai, T. Peng, J. Mao and L. Zan, *ACS Catal.*, 2013, **3**, 170–177.
74 J. S. Jang, S. J. Hong, J. Y. Kim and J. S. Lee, *Chem. Phys. Lett.*, 2009, **475**, 78–81.
75 P. Zeng, X. Zhang, X. Zhang, B. Chai and T. Peng, *Chem. Phys. Lett.*, 2011, **503**, 262–265.
76 H. Yu, Y. Zhao, C. Zhou, L. Shang, Y. Peng, Y. Cao, L.-Z. Wu, C.-H. Tung and T. Zhang, *J. Mater. Chem. A*, 2014, **2**, 3344–3351.
77 H. Yu, Y. Zhao, C. Zhou, L. Shang, Y. Peng, Y. Cao, L.-Z. Wu, C.-H. Tung and T. Zhang, *J. Mater. Chem. A*, 2014, **2**, 3344–3351.
78 Y. Ou, J. Lin, S. Fang and D. Liao, *Chem. Phys. Lett.*, 2006, **429**, 199–203.
79 Q. Xiang, J. Yu and M. Jaroniec, *Nanoscale*, 2011, **3**, 3670–3678.
80 Y. Wang, J. Yu, W. Xiao and Q. Li, *J. Mater. Chem. A*, 2014, **2**, 3847–3855.
81 P. Brown and P. V. Kamat, *J. Am. Chem. Soc.*, 2008, **130**, 8890–8891.
82 X.-Y. Zhang, H.-P. Li, X.-L. Cui and Y. Lin, *J. Mater. Chem.*, 2010, **20**, 2801–2806.
83 Z. Bian, T. Tachikawa, P. Zhang, M. Fujitsuka and T. Majima, *J. Am. Chem. Soc.*, 2013, **136**, 458–465.
84 M.-H. Pham, C.-T. Dinh, G.-T. Vuong, N.-D. Ta and T.-O. Do, *Phys. Chem. Chem. Phys.*, 2014, **16**, 5937–5941.
85 D. Jing and L. Guo, *Catal. Commun.*, 2007, **8**, 795–799.
86 D. Jing and L. Guo, *J. Phys. Chem. B*, 2006, **110**, 11139–11145.
87 N. Bao, L. Shen, T. Takata and K. Domen, *Chem. Mater.*, 2007, **20**, 110–117.
88 J. Cao, J. Z. Sun, J. Hong, H. Y. Li, H. Z. Chen and M. Wang, *Adv. Mater.*, 2004, **16**, 84–87.

89 X. Wang, G. Liu, G. Q. Lu and H.-M. Cheng, *Int. J. Hydrogen Energy*, 2010, **35**, 8199–8205.
90 G. Qing Lu, *Chem. Commun.*, 2009, 3452–3454.
91 J. Hou, Z. Wang, W. Kan, S. Jiao, H. Zhu and R. Kumar, *J. Mater. Chem.*, 2012, **22**, 7291–7299.
92 X. Zou, P.-P. Wang, C. Li, J. Zhao, D. Wang, T. Asefa and G.-D. Li, *J. Mater. Chem. A*, 2014, **2**, 4682–4689.
93 X.-H. Lu, S.-L. Xie, T. Zhai, Y.-F. Zhao, P. Zhang, Y.-L. Zhang and Y.-X. Tong, *RSC Adv.*, 2011, **1**, 1207–1210.
94 X. Zou, P.-P. Wang, C. Li, J. Zhao, D. Wang, T. Asefa and G.-D. Li, *J. Mater. Chem. A*, 2014, **2**, 4682–4689.
95 X. Cui, Y. Wang, G. Jiang, Z. Zhao, C. Xu, Y. Wei, A. Duan, J. Liu and J. Gao, *RSC Adv.*, 2014, **4**, 15689–15694.
96 Z. Wang, J. Hou, C. Yang, S. Jiao and H. Zhu, *Chem. Commun.*, 2014, **50**, 1731–1734.
97 G. Yang, W. Yan, Q. Zhang, S. Shen and S. Ding, *Nanoscale*, 2013, **5**, 12432–12439.
98 Z. Shen, G. Chen, Y. Yu, Q. Wang, C. Zhou, L. Hao, Y. Li, L. He and R. Mu, *J. Mater. Chem.*, 2012, **22**, 19646–19651.
99 Y.-x. Pan, H. Zhuang, J. Hong, Z. Fang, H. Liu, B. Liu, Y. Huang and R. Xu, *ChemSusChem*, 2014, **7**, 2537–2544.
100 L. Wang and W. Wang, *CrystEngComm*, 2012, **14**, 3315–3320.
101 T. Kida, G. Guan and A. Yoshida, *Chem. Phys. Lett.*, 2003, **371**, 563–567.
102 J. Choi, S. Y. Ryu, W. Balcerski, T. Lee and M. R. Hoffmann, *J. Mater. Chem.*, 2008, **18**, 2371–2378.
103 S. Y. Ryu, J. Choi, W. Balcerski, T. K. Lee and M. R. Hoffmann, *Ind. Eng. Chem. Res.*, 2007, **46**, 7476–7488.
104 Z. Shen, G. Chen, Q. Wang, Y. Yu, C. Zhou and Y. Wang, *Nanoscale*, 2012, **4**, 2010–2017.
105 Z. Khan, T. R. Chetia and M. Qureshi, *Nanoscale*, 2012, **4**, 3543–3550.
106 U. Gupta, B. G. Rao, U. Maitra, B. E. Prasad and C. N. R. Rao, *Chem. – Asian J.*, 2014, **9**, 1311–1315.
107 W. Zhang, Z. Zhong, Y. Wang and R. Xu, *J. Phys. Chem. C*, 2008, **112**, 17635–17642.
108 L. Ren, F. Yang, Y.-R. Deng, N.-N. Yan, S. Huang, D. Lei, Q. Sun and Y. Yu, *Int. J. Hydrogen Energy*, 2010, **35**, 3297–3305.
109 W. Zhang, Z. Zhong, Y. Wang and R. Xu, *J. Phys. Chem. C*, 2008, **112**, 17635–17642.
110 M. Liu, L. Wang, G. M. Lu, X. Yao and L. Guo, *Energy Environ. Sci.*, 2011, **4**, 1372–1378.
111 J. F. Reber and M. Rusek, *J. Phys. Chem.*, 1986, **90**, 824–834.
112 A. Deshpande, P. Shah, R. Gholap and N. M. Gupta, *J. Colloid Interface Sci.*, 2009, **333**, 263–268.
113 S. R. Lingampalli, U. K. Gautam and C. N. R. Rao, *Energy Environ. Sci.*, 2013, **6**, 3589–3594.
114 J. Hou, C. Yang, Z. Wang, S. Jiao and H. Zhu, *RSC Adv.*, 2012, **2**, 10330–10336.
115 X. Zong, H. Yan, G. Wu, G. Ma, F. Wen, L. Wang and C. Li, *J. Am. Chem. Soc.*, 2008, **130**, 7176–7177.
116 J. S. Jang, D. J. Ham, N. Lakshminarasimhan and J. S. Lee, *Appl. Catal., A*, 2008, **346**, 149–154.
117 W. Zhang, Y. Wang, Z. Wang, Z. Zhong and R. Xu, *Chem. Commun.*, 2010, **46**, 7631–7633.
118 H. Yan, J. Yang, G. Ma, G. Wu, X. Zong, Z. Lei, J. Shi and C. Li, *J. Catal.*, 2009, **266**, 165–168.
119 L. Yuliati, M. Kimi and M. Shamsuddin, *Beilstein J. Nanotechnol.*, 2014, **5**, 587–595.
120 T. Peng, P. Zeng, D. Ke, X. Liu and X. Zhang, *Energy Fuels*, 2011, **25**, 2203–2210.
121 Y. K. Kim and H. Park, *Energy Environ. Sci.*, 2011, **4**, 685–694.
122 J. Yu, B. Yang and B. Cheng, *Nanoscale*, 2012, **4**, 2670–2677.
123 L. Wang, Z. Yao, F. Jia, B. Chen and Z. Jiang, *Dalton Trans.*, 2013, **42**, 9976–9981.
124 X. Wang, M. Liu, Q. Chen, K. Zhang, J. Chen, M. Wang, P. Guo and L. Guo, *Int. J. Hydrogen Energy*, 2013, **38**, 13091–13096.
125 A. Ye, W. Fan, Q. Zhang, W. Deng and Y. Wang, *Catal. Sci. Technol.*, 2012, **2**, 969–978.
126 K. S. Novoselov, *Angew. Chem., Int. Ed.*, 2011, **50**, 6986–7002.
127 X.-J. Lv, W.-F. Fu, H.-X. Chang, H. Zhang, J.-S. Cheng, G.-J. Zhang, Y. Song, C.-Y. Hu and J.-H. Li, *J. Mater. Chem.*, 2012, **22**, 1539–1546.
128 J. Wang, P. Yang, J. Zhao and Z. Zhu, *Appl. Surf. Sci.*, 2013, **282**, 930–936.
129 Q. Li, H. Meng, J. Yu, W. Xiao, Y. Zheng and J. Wang, *Chem. – Eur. J.*, 2014, **20**, 1176–1185.
130 L. Jia, D.-H. Wang, Y.-X. Huang, A.-W. Xu and H.-Q. Yu, *J. Phys. Chem. C*, 2011, **115**, 11466–11473.
131 K. Chang, Z. Mei, T. Wang, Q. Kang, S. Ouyang and J. Ye, *ACS Nano*, 2014, **8**, 7078–7087.
132 J. Hou, C. Yang, H. Cheng, Z. Wang, S. Jiao and H. Zhu, *Phys. Chem. Chem. Phys.*, 2013, **15**, 15660–15668.
133 Q. Li, B. Guo, J. Yu, J. Ran, B. Zhang, H. Yan and J. R. Gong, *J. Am. Chem. Soc.*, 2011, **133**, 10878–10884.
134 J. Liu, H. Bai, Y. Wang, Z. Liu, X. Zhang and D. D. Sun, *Adv. Funct. Mater.*, 2010, **20**, 4175–4181.
135 T.-D. Nguyen-Phan, V. H. Pham, E. W. Shin, H.-D. Pham, S. Kim, J. S. Chung, E. J. Kim and S. H. Hur, *Chem. Eng. J.*, 2011, **170**, 226–232.
136 Q. Xiang, J. Yu and M. Jaroniec, *Chem. Soc. Rev.*, 2012, **41**, 782–796.
137 T. Peng, K. Li, P. Zeng, Q. Zhang and X. Zhang, *J. Phys. Chem. C*, 2012, **116**, 22720–22726.
138 Z. Yan, X. Yu, A. Han, P. Xu and P. Du, *J. Phys. Chem. C*, 2014, **118**, 22896–22903.
139 P. Zeng, Q. Zhang, T. Peng and X. Zhang, *Phys. Chem. Chem. Phys.*, 2011, **13**, 21496–21502.
140 X. Tang, Q. Tay, Z. Chen, Y. Chen, G. K. L. Goh and J. Xue, *J. Mater. Chem. A*, 2013, **1**, 6359–6365.
141 R. Lin, L. Shen, Z. Ren, W. Wu, Y. Tan, H. Fu, J. Zhang and L. Wu, *Chem. Commun.*, 2014, **50**, 8533–8535.

142 Y. Li, H. Wang and S. Peng, *J. Phys. Chem. C*, 2014, **118**, 19842–19848.
143 J. Zhang, J. Yu, M. Jaroniec and J. R. Gong, *Nano Lett.*, 2012, **12**, 4584–4589.
144 F. Schedin, A. Geim, S. Morozov, E. Hill, P. Blake, M. Katsnelson and K. Novoselov, *Nat. Mater.*, 2007, **6**, 652–655.
145 X. Wang, L. Yin and G. Liu, *Chem. Commun.*, 2014, **50**, 3460–3463.
146 P. Zeng, Q. Zhang, T. Peng and X. Zhang, *Phys. Chem. Chem. Phys.*, 2011, **13**, 21496–21502.
147 W. Tu, Y. Zhou and Z. Zou, *Adv. Funct. Mater.*, 2013, **23**, 4996–5008.
148 S. Bai and X. Shen, *RSC Adv.*, 2012, **2**, 64–98.
149 L. Amirav and A. P. Alivisatos, *J. Phys. Chem. Lett.*, 2010, **1**, 1051–1054.
150 T. Kida, G. Guan, Y. Minami, T. Ma and A. Yoshida, *J. Mater. Chem.*, 2003, **13**, 1186–1191.
151 J. Zhang, S. Z. Qiao, L. Qi and J. Yu, *Phys. Chem. Chem. Phys.*, 2013, **15**, 12088–12094.
152 X. Wang, W.-c. Peng and X.-y. Li, *Int. J. Hydrogen Energy*, 2014, **39**, 13454–13461.
153 J. Zhang, W. Zhu and X. Liu, *Dalton Trans.*, 2014, **43**, 9296–9302.
154 Y. Peng, Z. Guo, J. Yang, D. Wang and W. Yuan, *J. Mater. Chem. A*, 2014, **2**, 6296–6300.
155 M. Khatamian, M. Saket Oskoui and M. Haghighi, *New J. Chem.*, 2014, **38**, 1684–1693.
156 R. Peng, C.-M. Wu, J. Baltrusaitis, N. M. Dimitrijevic, T. Rajh and R. T. Koodali, *Chem. Commun.*, 2013, **49**, 3221–3223.
157 R. Peng, D. Zhao, J. Baltrusaitis, C.-M. Wu and R. T. Koodali, *RSC Adv.*, 2012, **2**, 5754–5767.
158 Z. Liu, S. Shen and L. Guo, *Int. J. Hydrogen Energy*, 2012, **37**, 816–821.
159 J. S. Jang, D. W. Hwang and J. S. Lee, *Catal. Today*, 2007, **120**, 174–181.
160 L. Ge, F. Zuo, J. Liu, Q. Ma, C. Wang, D. Sun, L. Bartels and P. Feng, *J. Phys. Chem. C*, 2012, **116**, 13708–13714.
161 J. S. Jang, S. M. Ji, S. W. Bae, H. C. Son and J. S. Lee, *J. Photochem. Photobiol., A*, 2007, **188**, 112–119.
162 J. S. Jang, H. G. Kim, U. A. Joshi, J. W. Jang and J. S. Lee, *Int. J. Hydrogen Energy*, 2008, **33**, 5975–5980.
163 Y. Chen, L. Wang, G. M. Lu, X. Yao and L. Guo, *J. Mater. Chem.*, 2011, **21**, 5134–5141.
164 C. Li, J. Yuan, B. Han, L. Jiang and W. Shangguan, *Int. J. Hydrogen Energy*, 2010, **35**, 7073–7079.
165 C. Xing, D. Jing, M. Liu and L. Guo, *Mater. Res. Bull.*, 2009, **44**, 442–445.
166 Y. J. Zhang, Y. C. Wang, W. Yan, T. Li, S. Li and Y. R. Hu, *Appl. Surf. Sci.*, 2009, **255**, 9508–9511.
167 C. Xing, D. Jing, M. Liu and L. Guo, *Mater. Res. Bull.*, 2009, **44**, 442–445.
168 T. T. D. Vu, F. Mighri, A. Ajji and T.-O. Do, *Ind. Eng. Chem. Res.*, 2014, **53**, 3888–3897.
169 H. N. Kim, T. W. Kim, I. Y. Kim and S. J. Hwang, *Adv. Funct. Mater.*, 2011, **21**, 3111–3118.
170 T. C. Dinh, M.-H. Pham, Y. Seo, F. Kleitz and T.-O. Do, *Nanoscale*, 2014, **6**, 4819–4829.
171 D. He, M. Chen, F. Teng, G. Li, H. Shi, J. Wang, M. Xu, T. Lu, X. Ji and Y. Lv, *Superlattices Microstruct.*, 2012, **51**, 799–808.
172 L. Qi, J. Yu and M. Jaroniec, *Phys. Chem. Chem. Phys.*, 2011, **13**, 8915–8923.
173 H. N. Kim, T. W. Kim, I. Y. Kim and S.-J. Hwang, *Adv. Funct. Mater.*, 2011, **21**, 3111–3118.
174 D. He, M. Chen, F. Teng, G. Li, H. Shi, J. Wang, M. Xu, T. Lu, X. Ji, Y. Lv and Y. Zhu, *Superlattices Microstruct.*, 2012, **51**, 799–808.
175 C.-T. Dinh, M.-H. Pham, F. Kleitz and T.-O. Do, *J. Mater. Chem. A*, 2013, **1**, 13308–13313.
176 T. D. Nguyen, C. T. Dinh and T. O. Do, *Chem. Commun.*, 2015, **51**, 624–635.
177 H. Park, Y. K. Kim and W. Choi, *J. Phys. Chem. C*, 2011, **115**, 6141–6148.
178 M. Khatamian, M. Saket Oskoui, M. Haghighi and M. Darbandi, *Int. J. Energy Res.*, 2014, **38**, 1712–1726.
179 Y. Chen and L. Guo, *J. Mater. Chem.*, 2012, **22**, 7507–7514.
180 H. Park, W. Choi and M. R. Hoffmann, *J. Mater. Chem.*, 2008, **18**, 2379–2385.
181 Y. Zhang, Y. Tang, X. Liu, Z. Dong, H. H. Hng, Z. Chen, T. C. Sum and X. Chen, *Small*, 2013, **9**, 996–1002.
182 M. de Oliveira Melo and L. A. Silva, *J. Photochem. Photobiol., A*, 2011, **226**, 36–41.
183 J. S. Jang, H. G. Kim, U. A. Joshi, J. W. Jang and J. S. Lee, *Int. J. Hydrogen Energy*, 2008, **33**, 5975–5980.
184 J. S. Jang, W. Li, S. H. Oh and J. S. Lee, *Chem. Phys. Lett.*, 2006, **425**, 278–282.
185 M. S. Oskoui, M. Khatamian, M. Haghighi and A. Yavari, *RSC Adv.*, 2014, **4**, 19569–19577.
186 J. Fang, L. Xu, Z. Zhang, Y. Yuan, S. Cao, Z. Wang, L. Yin, Y. Liao and C. Xue, *ACS Appl. Mater. Interfaces*, 2013, **5**, 8088–8092.
187 X.-F. Wu, H.-Y. Song, J.-M. Yoon, Y.-T. Yu and Y.-F. Chen, *Langmuir*, 2009, **25**, 6438–6447.
188 Y. Wang, X. Wang and M. Antonietti, *Angew. Chem., Int. Ed.*, 2012, **51**, 68–89.
189 X. Wang, K. Maeda, A. Thomas, K. Takanabe, G. Xin, J. M. Carlsson, K. Domen and M. Antonietti, *Nat. Mater.*, 2009, **8**, 76–80.
190 S. Cao and J. Yu, *J. Phys. Chem. Lett.*, 2014, **5**, 2101–2107.
191 Z. Zhao, Y. Sun and F. Dong, *Nanoscale*, 2015, **7**, 15–37.
192 B. Chai, T. Peng, J. Mao, K. Li and L. Zan, *Phys. Chem. Chem. Phys.*, 2012, **14**, 16745–16752.
193 H. W. Kang, S. N. Lim, D. Song and S. B. Park, *Int. J. Hydrogen Energy*, 2012, **37**, 11602–11610.
194 Q. Xiang, J. Yu and M. Jaroniec, *J. Phys. Chem. C*, 2011, **115**, 7355–7363.
195 Z. Xing, Z. Chen, X. Zong and L. Wang, *Chem. Commun.*, 2014, **50**, 6762–6764.

196 Y. Chen, J. Li, Z. Hong, B. Shen, B. Lin and B. Gao, *Phys. Chem. Chem. Phys.*, 2014, **16**, 8106–8113.
197 Z. Chen, P. Sun, B. Fan, Z. Zhang and X. Fang, *J. Phys. Chem. C*, 2014, **118**, 7801–7807.
198 Z. Jiang, D. Liu, D. Jiang, W. Wei, K. Qian, M. Chen and J. Xie, *Dalton Trans.*, 2014, **43**, 13792–13802.
199 H. Katsumata, Y. Tachi, T. Suzuki and S. Kaneco, *RSC Adv.*, 2014, **4**, 21405–21409.
200 J. Chen, S. Shen, P. Guo, P. Wu and L. Guo, *J. Mater. Chem. A*, 2014, **2**, 4605–4612.
201 D. Jiang, L. Chen, J. Xie and M. Chen, *Dalton Trans.*, 2014, **43**, 4878–4885.
202 L. Ge and C. Han, *Appl. Catal., B*, 2012, **117–118**, 268–274.
203 F. He, G. Chen, Y. Yu, S. Hao, Y. Zhou and Y. Zheng, *ACS Appl. Mater. Interfaces*, 2014, **6**, 7171–7179.
204 X. Zhang, L. Yu, C. Zhuang, T. Peng, R. Li and X. Li, *ACS Catal.*, 2013, **4**, 162–170.
205 H. Yan and Y. Huang, *Chem. Commun.*, 2011, **47**, 4168–4170.
206 S. Samanta, S. Martha and K. Parida, *ChemCatChem*, 2014, **6**, 1453–1462.
207 J. Hong, Y. Wang, Y. Wang, W. Zhang and R. Xu, *ChemSusChem*, 2013, **6**, 2263–2268.
208 Q. Li, B. Yue, H. Iwai, T. Kako and J. Ye, *J. Phys. Chem. C*, 2010, **114**, 4100–4105.
209 N. Bao, L. Shen, T. Takata, D. Lu and K. Domen, *Chem. Lett.*, 2006, 35.
210 H. Liu, J. Yang, J. Liang, Y. Huang and C. Tang, *J. Am. Ceram. Soc.*, 2008, **91**, 1287–1291.
211 Z. Jiang, F. Yang, N. Luo, B. T. Chu, D. Sun, H. Shi, T. Xiao and P. P. Edwards, *Chem. Commun.*, 2008, 6372–6374.
212 J. Jitputti, S. Pavasupree, Y. Suzuki and S. Yoshikawa, *Jpn. J. Appl. Phys.*, 2008, **47**, 751.
213 Y. Li, T. Sasaki, Y. Shimizu and N. Koshizaki, *J. Am. Chem. Soc.*, 2008, **130**, 14755–14762.
214 W. W. Wang, Y. J. Zhu and L. X. Yang, *Adv. Funct. Mater.*, 2007, **17**, 59–64.
215 E. C. Carroll, O. C. Compton, D. Madsen, F. E. Osterloh and D. S. Larsen, *J. Phys. Chem. C*, 2008, **112**, 2394–2403.
216 C. Ye, Y. Bando, G. Shen and D. Golberg, *J. Phys. Chem. B*, 2006, **110**, 15146–15151.
217 F. Andrew Frame, E. C. Carroll, D. S. Larsen, M. Sarahan, N. D. Browning and F. E. Osterloh, *Chem. Commun.*, 2008, 2206–2208, DOI: 10.1039/B718796C.
218 D. Jing, R. Li, M. Liu and L. Guo, *Int. J. Nanotechnol.*, 2011, **8**, 446–457.
219 J. Lv, T. Kako, Z. Li, Z. Zou and J. Ye, *J. Phys. Chem. C*, 2010, **114**, 6157–6162.
220 H. Gyu Kim, J. Suk Jang, E. Duck Jeong, Y. Jae Suh and J. Sung Lee, *Chem. Commun.*, 2009, 5889–5891.
221 A. C. Pradhan, S. Martha, S. Mahanta and K. Parida, *Int. J. Hydrogen Energy*, 2011, **36**, 12753–12760.
222 P. Dhanasekaran, H. G. Salunke and N. M. Gupta, *J. Phys. Chem. C*, 2012, **116**, 12156–12164.
223 A. Tanaka, K. Hashimoto and H. Kominami, *J. Am. Chem. Soc.*, 2013, **136**, 586–589.
224 Y. Luo, X. Liu, X. Tang, Y. Luo, Q. Zeng, X. Deng, S. Ding and Y. Sun, *J. Mater. Chem. A*, 2014, **2**, 14927–14939.
225 W. Xitao, L. Rong and W. Kang, *J. Mater. Chem. A*, 2014, **2**, 8304–8313.
226 Q. Jia, A. Iwase and A. Kudo, *Chem. Sci.*, 2014, **5**, 1513–1519.
227 S. Martha, K. H. Reddy and K. M. Parida, *J. Mater. Chem. A*, 2014, **2**, 3621–3631.
228 Y. Jia, S. Shen, D. Wang, X. Wang, J. Shi, F. Zhang, H. Han and C. Li, *J. Mater. Chem. A*, 2013, **1**, 7905–7912.
229 K. H. Reddy, S. Martha and K. M. Parida, *RSC Adv.*, 2012, **2**, 9423–9436.
230 K. M. Parida, A. Nashim and S. K. Mahanta, *Dalton Trans.*, 2011, **40**, 12839–12845.
231 J. Liu, H. Zhang, D. Tang, X. Zhang, L. Yan, Y. Han, H. Huang, Y. Liu and Z. Kang, *ChemCatChem*, 2014, **6**, 2634–2641.
232 T. Zhu, C. K. Nuo Peh, M. Hong and G. W. Ho, *Chem. – Eur. J.*, 2014, **20**, 11505–11510.
233 G. Tian, Y. Chen, Z. Ren, C. Tian, K. Pan, W. Zhou, J. Wang and H. Fu, *Chem. – Asian J.*, 2014, **9**, 1291–1297.
234 A. Nashim, S. Martha and K. M. Parida, *ChemCatChem*, 2013, **5**, 2352–2359.
235 W. Cui, D. Guo, L. Liu, J. Hu, D. Rana and Y. Liang, *Catal. Commun.*, 2014, **48**, 55–59.
236 L. Xu, L. Ni, W. Shi and J. Guan, *Chin. J. Catal.*, 2012, **33**, 1101–1108.

